

1 **Emerging Trends in Global Freshwater Availability**

2
3
4 **Authors:**

5
6
7 **M. Rodell^a, J.S. Famiglietti^b, D.N. Wiese^b, J.T. Reager^b, H.K. Beaudoin^{a,c}, F.W.**
8 **Landerer^b, and M.-H. Lo^d**

9
10
11 ^aHydrological Sciences Laboratory, NASA Goddard Space Flight Center, Greenbelt,
12 Maryland, USA

13 ^bJet Propulsion Laboratory, California Institute of Technology, Pasadena, California,
14 USA

15 ^cEarth System Science Interdisciplinary Center, University of Maryland, College Park,
16 Maryland, USA

17 ^dDepartment of Atmospheric Sciences, National Taiwan University, Taipei, Taiwan

18
19
20 Corresponding Author:

21 Matthew Rodell

22 +1 301-286-9143

23 Matthew.Rodell@nasa.gov
24
25
26

27 **Summary**

28

29 Freshwater availability is changing worldwide. Here we quantify 34 trends in
30 terrestrial water storage (TWS) observed by the Gravity Recovery and Climate Experiment
31 (GRACE) satellites during 2002-2016 and categorize their drivers as natural interannual
32 variability, unsustainable groundwater consumption, or climate change. Several of these
33 trends had been lacking thorough investigation and attribution, including massive changes
34 in northwestern China and the Okavango delta. Others are consistent with climate model
35 predictions. This observation-based assessment of how the world's water landscape is
36 responding to human impacts and climate variations provides a blueprint for evaluating
37 and predicting emerging threats to water and food security.

38

39 **Main Text**

40

41 Groundwater, soil moisture, surface waters, snow, and ice are dynamic components of
42 the terrestrial water cycle^{1,2,3}. They are not static on an annual basis (as early water budget
43 analyses supposed), yet absent hydroclimatic shifts or significant anthropogenic stresses
44 they typically remain range-bound. Recent studies have identified locations where
45 terrestrial water storage (TWS; the sum of these five components) appears to be trending
46 below previous ranges, notably where ice sheets or glaciers are diminishing in response to
47 climate change^{4,5} and where groundwater is being withdrawn at an unsustainable rate^{6,7,8}.

48 Accurate accounting of changes in freshwater availability is essential for predicting
49 regional food supplies, human and ecosystem health, energy generation, and social unrest.
50 Groundwater is particularly difficult to monitor and manage because aquifers are vast and
51 unseen, yet groundwater meets the domestic needs of roughly half of the world's

52 population⁹ and boosts food supply by providing for 38% of global consumptive irrigation
53 water usage¹⁰. Nearly two-thirds of terrestrial aquatic habitats are being increasingly
54 threatened¹¹ while the precipitation and river discharge that support them are becoming
55 more variable¹². A recent study¹¹ estimates that almost 5 billion people live in areas where
56 threats to water security are likely, a situation that will only be exacerbated by climate
57 change, population growth, and human activities. The key environmental challenge of the
58 21st century then may well be one of globally-sustainable water resources management.

59 Much of our knowledge of past and current freshwater availability comes from a
60 limited set of ground-based, point observations. Assessing changes in hydrologic
61 conditions at the global scale is exceedingly difficult using in situ measurements alone, due
62 to the cost of installing and maintaining instrument networks, gaps in those networks, and
63 a lack of digitization and sharing of what data do exist¹³. Satellite remote sensing has
64 proven crucial to monitoring water storage and fluxes in a changing world, enabling a truly
65 global perspective that spans political boundaries¹⁴. In particular, since its launch in 2002,
66 the GRACE mission¹⁵ has tracked ice sheet and glacier ablation, groundwater depletion,
67 and other TWS changes^{16, 17, 18, 19}. On a monthly basis GRACE can resolve TWS changes
68 with sufficient accuracy over scales that approximately range from 200,000 km² at low
69 latitudes to 90,000 km² near the poles¹. However, due to GRACE's coarse spatial
70 resolution, inability to partition component mass changes, and the brevity of the time series,
71 proper attribution of the TWS changes requires comprehensive examination of all available
72 auxiliary information and data, which has never before been performed at the global scale.

73 Here we map TWS change rates around the globe based on 14 years (April 2002 –
74 March 2016) of GRACE observations (Figure 1). The GRACE data were processed using

75 an advanced mass concentration²⁰ (“mascon”) approach that enables improved signal
76 resolution relative to the standard spherical harmonic technique²¹. Best fit linear rates of
77 change after removing the seasonal cycle (referred to herein as “apparent trends”) are
78 presented in Table 1 for 34 study regions. For context, the largest man-made reservoir in
79 the U.S., Lake Mead, has a capacity of about 32 Gt; during the study period all but one of
80 the 34 regions lost or gained more water than that and eleven of them lost or gained more
81 than ten times that amount. The reported uncertainty bounds are typically low because
82 error in the removal of glacial isostatic adjustment (GIA) signals is the only major source
83 of noise in the secular signal; low uncertainty does not, on its own, imply that the apparent
84 trends existed before the GRACE period or will continue into the future. The coefficient
85 of determination (r^2), representing the “goodness of fit” of the regressed linear trends, is
86 included in Table 1 to quantify the strength of the apparent trends relative to non-secular
87 interannual variability. It is hence a useful but by no means conclusive piece of evidence
88 for predicting whether the trend will be fleeting or enduring, reflecting the cohesiveness of
89 the TWS time series tendencies in Figures ED1-ED4. We attribute the trends to natural
90 variability, direct human impacts, or climate change and forecast the likelihood that they
91 will continue based on 1979-2016 precipitation data from the Global Precipitation
92 Climatology Project version 2.3 (GPCP)²² (see Figures ED5-ED8), an irrigated area map²³,
93 satellite-based lake level altimetry time series²⁴, Landsat imagery, and published reports of
94 human activities including agriculture, mining, reservoir operations, and inter-basin water
95 transfers. Further, for each region we provide the median climate model prediction of
96 precipitation changes between 1986-2005 and 2081-2100, under the Representative
97 Concentration Pathways 8.5 W/m² (RCP8.5; “business as usual”) greenhouse gas

98 emissions scenario from the Intergovernmental Panel on Climate Change (IPCC) Fifth
99 Assessment Report²⁵. We chose the high-end scenario because it accentuates regional
100 differences, which are more important for this analysis than absolute magnitudes. Figure
101 2 presents maps of the IPCC, GPCP, and irrigated area data.

102

103 **Global Scale**

104 By far the largest TWS trends occur in Antarctica (region 1; -127.6 ± 39.9 Gt/yr
105 averaged over the continent), Greenland (region 2; -279.0 ± 23.2 Gt/yr), the gulf coast of
106 Alaska (region 3; -62.6 ± 8.2 Gt/yr), and the Canadian archipelago (region 4; -74.6 ± 4.1
107 Gt/yr), where the warming climate continues to drive rapid ice sheet and glacier ablation⁴,
108 ^{5, 26, 27}. Positive trends in sub-regions of Antarctica and Greenland result from increasing
109 snow accumulation²⁸ and millennial-scale dynamic thickening processes^{29, 30}. Excluding
110 those four ice-covered regions, one of the most striking aspects of changing TWS
111 illuminated by Figure 1 is that freshwater seems to be accumulating in far northern North
112 America (region 5) and Eurasia (region 6) and in the wet tropics, while the greatest non-
113 frozen freshwater losses have occurred at mid-latitudes^{8, 31}. The observed trends are
114 consistent with increasing rates of precipitation during the period and the prediction of
115 IPCC models that precipitation generally will decrease in mid-latitudes and increase in low
116 and high latitudes by the end of this century²⁵. They also complement recent studies that
117 identify increasing rates of precipitation in the tropics and increasing water storage and
118 river discharge in the high Arctic^{12, 32}. However, because the rates of TWS change (0.45
119 ± 0.43 cm/yr and 0.17 ± 0.12 cm/yr in regions 5 and 6) and coefficients of determination

120 (0.52 and 0.10) are small, while GIA related errors are relatively large, we cannot state
121 definitively that these high latitude tendencies are real trends.

122 A second distinguishing characteristic of the map is that it reveals a clear ‘human
123 fingerprint’ on the global water cycle. As seen in Figure 2, freshwater is rapidly
124 disappearing in many of the world’s irrigated agricultural regions^{6, 10, 33, 34, 35, 36, 37, 38}. A
125 third aspect of the global trend map is natural interannual variability; many of the apparent
126 trends are likely to be temporary, caused by oscillations between dry and wet periods
127 (themselves driven by El Nino / La Nina and other climatic cycles) during the 14-year
128 study period^{39, 40}.

129

130 **Eurasia**

131 The hotspot in northern India (region 7) was among the first non-polar TWS trends to
132 be revealed by GRACE^{41, 42}. It results from groundwater extraction to irrigate crops
133 including wheat and rice in a semi-arid climate. Fifty-four percent of the area is equipped
134 for irrigation. We estimate the rate of TWS depletion to be 19.2 ± 1.1 Gt/yr, which is within
135 the range of GRACE based estimates from previous studies of differently-defined northern
136 India regions^{41, 42, 43}. The trend persists despite precipitation being 101% of normal
137 (compared with the 1979-2015 GPCP annual mean for the region) during the study period,
138 with an increasing trend of 15.8 mm/yr. That extractions already exceed recharge during
139 normal years does not bode well for groundwater during future droughts. The contribution
140 of Himalayan glacier mass loss to the regional trend is minor^{41, 42}.

141 The increasing trend in central and southern India (region 8; 9.4 ± 0.6 Gt/yr) likely
142 reflects natural variability of (mostly monsoon) precipitation, which was 104% of normal

143 with an increasing rate of 3.7 mm/yr (0.4%/yr). The r^2 value is low (0.24), yet both trends
144 are consistent with the IPCC-RCP8.5 predicted 23% precipitation increase by 2100.

145 The increasing trend in east-central China (region 9) is caused by a surge in dam
146 construction and subsequent reservoir filling across that region⁴⁴. Best known is the Three
147 Gorges Dam Reservoir, which was filled to its design capacity of 39.3 Gt between June
148 2003 and October 2010⁴⁵. The 14-year regional trend, 7.8 ± 1.6 Gt/yr, did not change
149 appreciably after the Three Gorges Dam Reservoir was filled. That can be explained by
150 both the prevalence of other dam projects and greater precipitation after 2010 (971 mm/yr)
151 than before (928 mm/yr). Further, seepage from dams tends to raise the regional water
152 table, which can continue for years before the system equilibrates⁴⁶. If precipitation trends
153 towards an 8% increase by the end of this century, as predicted, then the observed TWS
154 trend may persist even after the current dam building boom, though probably at a slower
155 pace.

156 Satellite altimetry and Landsat data indicate that the majority of lakes in the Tibetan
157 Plateau have grown in water level and extent during the 2000s, owing to a combination of
158 elevated precipitation rates and increased glacier melt flows⁴⁷ that is difficult to
159 disentangle. From 1997 to 2001 the average annual precipitation in region 10 was 160
160 mm/yr, well below the 2002-2015 average of 175 mm/yr, thus the observed increase in
161 TWS (7.7 ± 1.4 Gt/yr) may reflect replenishment after a prolonged dry period. Additional
162 surface water storage would have been partially offset by glacier retreat and warming-
163 enhanced evaporation. GIA may further complicate the partitioning of the GRACE derived
164 mass change signal over the Tibetan Plateau⁴⁸, but some have argued that the GIA
165 contribution is negligible⁴⁹. The latter study noted that interannual mass variability in the

166 region during the GRACE period is large relative to the inferred trend⁴⁹. We concur ($r^2 =$
167 0.67) and conclude that there is no basis to extrapolate the apparent TWS trend into the
168 future. In fact, it appears to have reversed in 2013 (Figure ED2). Although IPCC-RCP8.5
169 predicts a 20% increase in precipitation by 2100, it is probable that warming-induced
170 glacier mass losses will begin to exceed surface water gains, particularly if the fraction of
171 frozen precipitation decreases.

172 Region 11 lies to the west of the city of Urumqi in northwestern China's Xinjiang
173 province. During the study period TWS depletion was intense: -5.5 ± 0.5 Gt/yr from an
174 area of only 215,000 km². Precipitation data indicate drought was a nonfactor. The glaciers
175 of the Tien Shan mountain range, whose central third lies within region 11, are melting
176 rapidly⁴⁹, but not rapidly enough to explain all of the mass loss. Groundwater is being
177 withdrawn to support irrigated agriculture across the province^{50, 51} and possibly to dewater
178 coal mines⁵². However, region 11 is contained within an endorheic basin. Hence the
179 additional surface water produced by ice melt and groundwater abstraction cannot flow far,
180 yet the elevations of the five lakes within that basin either declined or were stable during
181 the study period, and GRACE did not detect significant TWS increases in other parts of
182 the basin. We conclude that region 11 is losing glacier ice and possibly groundwater which
183 ultimately become evapotranspiration, both in irrigated agricultural areas to the north,
184 south, and west of the mountains and as evaporation from the desert floor to the south⁵⁰.
185 Details are provided in the supplementary Methods.

186 The vast agricultural region surrounding Beijing (region 12) is heavily irrigated (52%).
187 Previous GRACE-based studies offered a wide range of estimates of groundwater depletion
188 from the North China Plain aquifer (see the supplementary Methods for details), which is

189 encompassed by region 12 and supports much of that irrigation. Here we estimate a TWS
190 change rate of -11.3 ± 1.3 Gt/yr for region 12. During the GRACE period annual total
191 precipitation held steady, about 10 mm/yr above the 1979-2015 mean, following two dry
192 years and a wet year during 2001-2003. All evidence suggests that this trend is human
193 induced and likely to continue until groundwater becomes scarce or regulations are put in
194 place to reduce consumption rates.

195 The negative trend that extends across East India, Bangladesh, Burma, and southern
196 China (region 13), -23.3 ± 1.9 Gt/yr, may be explained by a combination of intense
197 irrigation⁵³ (25%) and a decrease in monsoon season precipitation during the period.
198 Annual total precipitation was well above normal from 1998 to 2001, resulting in elevated
199 TWS. During the GRACE period, precipitation declined at a rate of -10 mm/yr ($-0.7\%/yr$),
200 and the annual accumulations were below average from 2009 to 2015. This is the third
201 most heavily irrigated of the study regions, so TWS decline is likely to continue, though
202 perhaps at a slower rate given that rainfall should normalize eventually and a 15% increase
203 in rainfall is predicted by 2100.

204 Decreasing water storage in the Middle East has been quantified using GRACE by
205 previous studies^{54, 55, 56}. Here we split the affected area into two regions, northwest Saudi
206 Arabia (region 14; -10.5 ± 1.5 Gt/yr) and the northern Middle East (region 15; including
207 eastern Turkey, Syria, Iraq, and Iran; -32.1 ± 1.5 Gt/yr). The declines result from a
208 combination of recent drought and consequent increases in groundwater demand. Average
209 precipitation during the study period was 78% and 96% of the 1979-2015 means in regions
210 14 and 15, with a slight declining trend ($-1\%/yr$) in both. While the irrigation dataset
211 indicates that less than 1% of region 14 is irrigated, Landsat imagery reveals the appearance

212 and expansion of crop irrigation over the past three decades, supplied by non-renewable
213 groundwater. However, the Saudi government ended their domestic wheat production
214 program in market year 2014-15⁵⁷. Thus while some farms have continued to operate, it is
215 likely that the depletion rate in region 14 will diminish, and TWS may already be
216 stabilizing (Figure ED2).

217 Region 15 has experienced a more complicated recent water history^{54, 58}. Turkey's
218 construction of 22 dams upstream on the Tigris and Euphrates Rivers in the last 3 decades
219 has significantly decreased the rate of flow into Iraq and Syria. Combined with long-term
220 drought, this has forced widespread over-reliance on groundwater for both domestic and
221 agricultural needs and largely explains the large negative TWS trend^{54, 59}. Surface and
222 groundwater depletion is likely to continue in a stepwise fashion, with periods of near-
223 stability during normal to wet years and rapid declines during drought years.

224 To the north, an adjoining zone of TWS depletion (region 16; -18.1 ± 1.3 Gt/yr) extends
225 from the Ukraine through western Russia and into Kazakhstan. As before, the root cause
226 is competition for scarce water resources, exacerbated by drought. Fifteen percent of the
227 area is irrigated, including fertile croplands that are vital to Russia. Precipitation during
228 the period was 97% of normal with a decreasing trend of 6 mm/yr (1%/yr). As in region
229 15, surface and groundwater depletion in region 16 is likely to continue as it has, stepwise,
230 with substantial declines during drought years (2008, 2012, and 2014) and lesser recoveries
231 in normal to wet years.

232 The water demands of regions 15 and 16 place severe pressure on the Aral and Caspian
233 Seas⁶⁰ (regions 17 and 18). The demise of the Aral Sea is well known. Our estimate of
234 the mass change in what remains of it is -2.2 ± 0.1 Gt/yr. Water level fluctuations in the

235 Caspian Sea have previously been attributed to meteorological variability⁸ and direct
236 evaporation from the Sea⁶¹. We find that annual discharge from the Volga River explains
237 60% of the variance in annual mean Caspian Sea level compared with 18% explained by
238 evaporation from the Sea. Interannual variations in Volga River discharge are nearly three
239 times as large as interannual variations in evaporation, and the former are controlled by
240 both precipitation changes and the water demands of crops that cover 37% of the basin.
241 Using crop production data and other information we establish that the -23.7 ± 4.2 Gt/yr
242 rate of change of water mass in the Caspian Sea observed by GRACE was caused in part
243 by diversions and direct withdrawals of water from the rivers that sustain it (see the
244 supplemental Methods for details), mirroring the circumstances that doomed the Aral Sea.
245 The Caspian Sea contains about 78,000 Gt of water, so at the current rate it will survive for
246 three more millennia, but a receding shoreline could be an issue.

247 Three mass changes that are prominent in Figure 1 in Eurasia are not associated with
248 TWS at all. Crustal deformation accompanying the 2004, magnitude 9.1 Sumatra-
249 Andaman earthquake caused two of the mass changes, the dipole positive and negative
250 trends in Sumatra and the Malay Peninsula, respectively⁶². The 2011, magnitude 9.0
251 Tohoku earthquake caused the negative trend in Japan⁶³.

252

253 **North America**

254 Ongoing GIA processes centered near Hudson Bay, where the Laurentide ice sheet was
255 thickest 20-95 thousand years ago, require a correction of the mass rates observed by
256 GRACE of up to 5-6 cm/yr (equivalent height of water)^{64, 65}. However, GIA models are
257 imperfect and thus there is large uncertainty in the apparent decreasing TWS trend in

258 central Canada (region 19) and some evidence that it may reflect an overcorrection of
259 GIA⁶⁶. Nevertheless, here we estimate the rate to be -7.0 ± 6.4 Gt/yr. Loss of water would
260 be consistent with a recent study that concluded Canada's subarctic lakes are vulnerable to
261 drying when snow cover declines, and that recent bouts of drying may be unprecedented
262 in the past 200 years⁶⁷. On the other hand, precipitation has been 102% of normal during
263 the GRACE period, and a 17% increase is predicted by the end of the century.

264 The wetting trend in the northern Great Plains (region 20), 20.2 ± 4.8 Gt/yr, arises from
265 a combination of deep drought during 2001 to 2003, which greatly depressed water levels
266 at the start of the GRACE period, followed by nine of the next eleven years having greater
267 than average precipitation, including flooding in 2010-11⁶⁸. The trend is likely to diminish
268 over time although a 7% increase in precipitation is predicted by 2100.

269 A historically severe drought centered in southern California (region 21) that began in
270 2007 (ignoring a wet 2010) and consequent increases in groundwater demand^{69, 70}
271 conspired to diminish TWS at a rate of -4.2 ± 0.4 Gt/yr. While atmospheric rivers during
272 2016-2017 replenished California's surface waters and policy changes have been enacted,
273 it is doubtful that aquifer storage will recover completely absent significant usage
274 reductions, in part because dewatering of aquifer materials can cause compaction of
275 sediments, reducing aquifer capacity irrevocably⁷¹. In the Central Valley, which accounts
276 for one third of the vegetables and two thirds of the fruits and nuts grown in the U.S.,
277 annual water demands for agriculture have exceeded renewable water resources since the
278 early 20th century⁷¹. Groundwater well observations that extend back to 1962 suggest that
279 each successive drought causes groundwater levels to step down to a new normal range
280 without full recovery⁷¹, as in regions 15 and 16. Declining winter snowpack in the Sierra

281 Nevada Mountains, including a 500-year low in 2015⁷², is a major concern because it is
282 the main source of the region's surface water supply and groundwater recharge.

283 Sporadic droughts⁷³ in region 22, which encompasses parts of the southern High Plains
284 and Texas, produced an apparent trend of -12.2 ± 3.6 Gt/yr during the GRACE period. In
285 this case we forecast partial replenishment. Large precipitation variations caused TWS to
286 seesaw between high and low (Figure ED7). Heavy rains that led to flooding in parts of
287 Texas and Oklahoma in May and October of 2015 and again in June of 2016 ended the
288 most recent drought and reduced the linear rate of TWS decline during the GRACE period.
289 On the other hand, withdrawals of groundwater that exceed recharge in the central and
290 southern High Plains aquifer, to support irrigated agriculture, have persisted for decades⁷⁴
291 and will continue until the resource is exhausted or management policies change. The
292 fringes of the aquifer have already run dry in places, and recent estimates predict that the
293 southern High Plains aquifer could be depleted within 30 years⁷⁴. Despite this situation,
294 entrenched water rights are likely to preserve the status quo until the damage forces the
295 hands of policymakers and stakeholders.

296

297 **South America**

298 Melting of the Patagonian ice fields (region 23) has previously been documented using
299 altimetry⁷⁵ and GRACE⁷⁶. Based on our analysis (see the supplemental Methods for
300 details), TWS loss is occurring at a rate of -25.7 ± 5.1 Gt/yr. In a warming world, melting
301 of the Patagonian ice fields will continue until they are exhausted.

302 The magnitude 8.8 Maule (Chile) earthquake that occurred on 27 February 2010 is
303 partly responsible for the apparent trend in Central Argentina⁷⁷ (region 24). A model has

304 not yet been developed to properly separate its effect from TWS variations after that date
305 (Figure ED3). TWS had previously been declining at a rate of -8.6 ± 1.2 Gt/yr. The region
306 received substantially elevated precipitation in five of the six years between 1999 and 2004,
307 producing a TWS surplus at the start of the GRACE period. Multi-year drought began in
308 2009, resulting in the observed April 2002 to February 2010 negative trend. TWS appears
309 to have begun recovering (Figure ED3) in response to above-normal precipitation in 2014
310 and 2015 (Figure ED7), and we envisage that it will return to mean wetness conditions
311 over time.

312 TWS increased during the GRACE period in central and western Brazil and its
313 neighbors (region 25) at a rate of 51.9 ± 9.4 Gt/yr. The region received less than average
314 rainfall in every year from 2001 to 2005, followed by greater than average rainfall in six
315 of the next ten years. As a result, TWS recovered from the early-period drought⁷⁸ and
316 exhibited a massive but transitory increasing trend which may have already ended (Figure
317 ED3). The magnitude is explained by both the size of the region and the intensity of the
318 Amazon water cycle⁷⁹. Still, we note that southern Brazil is a hotbed of dam construction⁴⁴,
319 and it is possible that the filling of reservoirs contributed to the upward trend. Eastern
320 Brazil (region 26) recently has suffered from a major drought⁸⁰, including well below
321 normal rainfall in 2012, 2014, and 2015, causing TWS to plunge at a mean rate of -16.7
322 ± 2.9 Gt/yr during the GRACE period. In both cases, assuming precipitation rates revert
323 towards (or oscillate around) their long term means, the observed trends should fade. In
324 fact, owing to the recent strong El Nino, 2015 was the driest year in the 37-year record for
325 region 25 (Figure ED7), which may portend a reversion to average TWS.

326

327 **Africa**

328 Six apparent trends stand out in Africa. In southern Africa, a powerful wetting trend,
329 29.5 ± 3.5 Gt/yr, encompasses the western Zambezi basin, the Okavango delta, and areas
330 west to the coast (region 27). This region experienced a remarkable change in its
331 hydroclimate. Area averaged annual rainfall was less than 970 mm in every year from
332 1979 to 2005. That threshold was exceeded five times from 2006 to 2011. A permanent
333 climatic shift was previously speculated based on a significant decrease in annual
334 precipitation between 1950-1975 and 1980-2005⁸¹. With ten years of additional hindsight,
335 it appears that the region may simply have endured a prolonged drought from the late 1970s
336 to the early 2000s. Thus, we attribute the GRACE period trend to natural variability⁸².
337 Though TWS appears to have peaked in 2012 (Figure ED4), considering that the previous
338 wet and dry periods lasted upwards of 25 years it is plausible that the wetting trend could
339 resume.

340 An apparent trend of 21.9 ± 3.9 Gt/yr occurs along the headwaters of the White Nile
341 and Blue Nile Rivers, including Lakes Tanganyika and Victoria (region 28). Altimetry
342 data indicate that during the study period both lakes experienced minimum water levels in
343 2006 and that their annual mean levels increased by 62 and 40 mm/yr on average, all of
344 which is consistent with the TWS time series. Together, the two lake level trends equate
345 to less than a quarter (4.8 Gt/yr) of the observed TWS trend. Considering that, rainfall
346 would seem to be the primary driver of TWS variations, while management of the large
347 lakes⁸³ and dam building in the northern part of the region⁸⁴ also contribute. However,
348 rainfall is not particularly well correlated with either TWS or lake levels. The lack of
349 correlation may be indicative of inaccuracies stemming from the sparsity of rain gauges in

350 the region. The observed rainfall trend was negligible during the period, but a 12% increase
351 is predicted by 2100. The northern part of region 28 encompasses the Grand Ethiopian
352 Renaissance Dam on the Blue Nile River at Ethiopia's northwest border with Sudan, which
353 Egypt has strongly denounced because of the possibility of reduced flow through the Nile.
354 Construction of the dam began in 2011 and is ongoing. Filling of the 74 km³ reservoir will
355 likely produce a temporary increasing TWS trend in its immediate vicinity.

356 TWS has been increasing in tropical western Africa (region 29) at a rate of 24.1 ±2.1
357 Gt/yr. Precipitation was 3% below normal in 2000-2002 and 3% above during the rest of
358 the GRACE period. This appears to be the primary cause of TWS accumulation, though
359 the possible contribution of the many dams being built in this part of Africa⁴⁴ is unknown.
360 Interannual variability of rainfall is substantial in the region⁸⁵, so disregarding the dams, it
361 is likely that the rate of change of TWS will oscillate around zero over the coming decades.
362 By 2100 rainfall is predicted to decrease by 6%, hence the dam construction may be timely.

363 Decreasing TWS (-7.2 ±1.0 Gt/yr) in region 30, which extends from the coast of central
364 Africa into the northern Congo River basin, seems to be caused by natural interannual
365 variability, though it has been suggested that the surface runoff rate has been enhanced by
366 deforestation⁸⁴. Between 1999 and 2002 rainfall averaged 4% above normal, while it
367 averaged 1% below normal during the rest of the GRACE period, including two very dry
368 years in 2014 and 2015. The decrease in TWS also happens to be consistent with the
369 postulated negative correlation between TWS in the Amazon and Congo basins⁸⁶, which
370 further implicates large scale climatic oscillation as the ultimate driver⁸⁵.

371 The negative trend along the coast of southeastern Africa (region 31), -12.9 ±2.3 Gt/yr,
372 reflects a recent severe drought⁷⁹ which has caused major food shortages. Rainfall was 4%

373 below average during the GRACE period, including annual accumulations that were below
374 normal in five of the last eight years and barely above normal in the other three. Water
375 levels in Lake Malawi, which is in the center of the region, are well correlated with regional
376 TWS. The lake declined at a mean rate of 78 mm/yr during the period, accounting for 2.3
377 Gt/yr of the observed TWS trend. Thus it is likely that the apparent trend is primarily
378 caused by natural variability⁸⁴, though a 6% decrease in rainfall is predicted during this
379 century.

380 A weak negative trend, -11.7 ± 2.9 Gt/yr, extends across arid Africa north of 19°N
381 excluding Morocco (region 32). The coefficient of determination is not large at 0.45,
382 nevertheless, precipitation during the GRACE period was 7% above normal, which
383 suggests that the consumptive use of fossil groundwater to stimulate agriculture and
384 economic development is the cause^{55, 84, 87}. Three studies^{6, 10, 36} estimated recent rates of
385 consumptive groundwater use across North Africa to be 7.8, 15.7, and 4.1 Gt/yr, bracketing
386 our TWS depletion estimate.

387

388 **Australia**

389 Australia appears to be bipolar with respect to water storage during the GRACE era,
390 with wetting in the east and north and drying in the northwest. The worst drought in over
391 100 years afflicted eastern Australia during 2001-09⁸⁸. It is likely that groundwater was
392 more heavily consumed during that time to compensate for reduced availability of surface
393 waters. Recovery from the drought began with heavy rains in 2010 and transitioned to
394 severe flooding in 2011, with so much water stored on the continent in 2012 that global
395 mean sea level temporarily declined⁸⁹. The shift from dry to wet conditions caused the

396 apparent wetting trend in region 33, 19.0 ± 2.8 Gt/yr, but most of that water had already
397 been shed by 2016 (Figure ED4). North Western Australia received greater than normal
398 rainfall during every year from 1997 to 2001, including the two wettest years in the GPCP
399 record in 2000 and 2001. Thus region 34 began 2002 near maximum TWS capacity, and
400 it gradually returned to average⁹⁰ (-8.9 ± 1.2 Gt/yr) with 99% of normal precipitation during
401 the GRACE period. It is possible that aquifer dewatering associated with Pilbara's mining
402 industry also contributed, but reliable data are not available to confirm and quantify that
403 contribution. We can only justifiably conclude that natural variability is the primary
404 explanation for both Australian trends.

405

406 **Implications and Discussion**

407 GRACE has revealed significant changes in freshwater resources occurring across the
408 globe, and has enabled them to be quantified at regional scales, unimpeded by sparse
409 measurements or restrictive data access policies. Some of these changes are manifestations
410 of human water management that, prior to GRACE, were known only anecdotally,
411 including TWS depletion in northern India, the north China plain, and the Middle East
412 (regions 7, 12, 14-16), or not at all, as in northwestern China (region 11). They portend a
413 future in which already limited water resources will become even more precious. Others
414 correlate well with global warming and predicted future precipitation changes, including
415 worldwide ice sheet and glacier melt (regions 1-4, 23) and TWS increases in the northern
416 high latitudes (regions 5-6). Apparent TWS trends in about one-third of the study regions
417 represent partial cycles of longer term interannual oscillations, and may well fade or
418 reverse over the decades (see green dots in Figure 1). While we have made every effort to

419 attribute the apparent trends properly, all will require continued observation to better
420 understand their causes and constrain their rates.

421 The GRACE data provide motivation for multilateral cooperation among nations,
422 states, and stakeholders, including development of transboundary water sharing
423 agreements, to balance competing demands and defuse potential conflict³³. Government
424 policies that incentivize water conservation could help to avert a “tragedy of the commons”
425 scenario, i.e., opportunistic competition for groundwater outweighing the altruistic impulse
426 to preserve the resource. Northern India, the North China Plain, the Middle East, and the
427 area surrounding the Caspian Sea are already on a perilous path, while California, in
428 response to severe drought and alarming groundwater declines in the Central Valley,
429 recently passed legislation to regulate groundwater consumption.

430 In many regions, crop irrigation on massive scales has been supported by unsustainable
431 rates of groundwater abstraction^{6, 33, 33, 34, 91}. In the face of aquifer depletion, population
432 growth, and climate change, water and food security will depend upon water saving
433 technologies and improved management and governance. The success of such an approach
434 in arid Israel⁹² proves that a comprehensive water conservation strategy can work, and there
435 are encouraging signs in Saudi Arabia (as previously discussed) and parts of India⁹³ as
436 well. Meanwhile, as China looks to improve living standards for its 1.38 billion residents,
437 it will continue to face daunting water management decisions, many related to massive
438 geoengineering and water diversion projects that are likely to trigger political tensions.

439 The GRACE data also call attention to regions where continued monitoring will be
440 essential for distinguishing, understanding, and quantifying climate change impacts on the
441 water cycle^{94, 95} and groundwater^{96, 97} in particular. This is important for two reasons. First,

442 verification of emerging hydroclimatic trends such as increasing northern high latitude
443 precipitation would raise confidence in the ability of climate models to predict water cycle
444 consequences of climate change⁹⁸. Second, a redistribution of freshwater from dry to wet
445 regions, as has been forecast, could exacerbate disparities between the water “haves” and
446 “have nots” and associated political instability, migration, and conflict. Most groundwater
447 depletion is occurring within Earth’s mid-latitudes, resulting in a positive drying feedback
448 that is accelerating water losses and the severity of related socioeconomic issues³³.

449 New and future satellite remote sensing missions that extend the long term record of
450 global, hydrological observations will be essential for continued assessment of changing
451 freshwater availability⁹⁹. In particular, the GRACE Follow On mission (planned to launch
452 in early 2018), while affording a small increase in spatial resolution/accuracy¹⁰⁰, will
453 enable surveillance of the trends described here and improved disentanglement of natural
454 TWS variability from hydroclimatic change. Awareness of changing freshwater
455 availability (e.g., Figure 1) is the first step towards addressing the challenges discussed
456 here, through improved infrastructure, water use efficiency, lifestyle and water
457 management decisions, and policy.

458

459 **References**

- 460 1. Changnon, S.A. Detecting drought conditions in Illinois. Circular 169 (Illinois State
461 Water Survey, 1987).
- 462 2. Rodell, M., & Famiglietti, J. S. An analysis of terrestrial water storage variations in
463 Illinois with implications for the Gravity Recovery and Climate Experiment
464 (GRACE). *Wat. Resour. Res.* **37**, 1327-1340, doi:10.1029/2000WR900306 (2001).
- 465 3. Getirana, A., Kumar, S., Giroto, M., & Rodell, M. Rivers and floodplains as key
466 components of global terrestrial water storage variability. *Geophys. Res. Lett.* **44**,
467 10359-10368, doi:10.1002/2017GL074684 (2017).

- 468 4. Luthcke, S. B. *et al.* Antarctica, Greenland and Gulf of Alaska land ice evolution
469 from an iterated GRACE global mascon solution. *J. Glac.* **59**, 613-631,
470 doi:10.3189/2013JoG12J147 (2013).
- 471 5. Velicogna, I., Sutterley, T. C., & van den Broeke, M. R. Regional acceleration in ice
472 mass loss from Greenland and Antarctica using GRACE time-variable gravity data.
473 *Geophys. Res. Lett.* **41**, 8130–8137, doi:10.1002/2014GL061052 (2014).
- 474 6. Wada, Y., van Beek, L. P. H., & Bierkens, M. F. P. Nonsustainable groundwater
475 sustaining irrigation: A global assessment. *Water Resour. Res.* **48**, W00L06,
476 doi:10.1029/2011WR010562 (2012).
- 477 7. Konikow, L.F. Contribution of global groundwater depletion since 1900 to sea-level
478 rise. *Geophys. Res. Lett.* **38**, L17401, doi:10.1029/2011GL048604 (2011).
- 479 8. Van Dijk, A.I.J.M., Renzullo, L.J., Wada, Y., & Tregoning, P. A global water cycle
480 reanalysis (2003–2012) merging satellite gravimetry and altimetry observations with
481 a hydrological multi-model ensemble. *Hydrol. Earth Syst. Sci.*, **18**, 2955–2973,
482 doi:10.5194/hess-18-2955-2014 (2014).
- 483 9. Zektser, I. S. & Everett, L. G. *Groundwater Resources of the World and Their Use.*
484 <http://unesdoc.unesco.org/images/0013/001344/134433e.pdf> (UNESCO, 2004).
- 485 10. Siebert, S. *et al.* Groundwater use for irrigation – a global inventory. *Hydrol. Earth*
486 *Syst. Sci.* **14**, 1863-1880, doi:10.5194/hess-14-1863-2010 (2010).
- 487 11. Vörösmarty, C. J. *et al.* Global threats to human water security and river biodiversity.
488 *Nature* **467**, 555-561, doi:10.1038/nature09440 (2010).
- 489 12. Syed, T. H., Famiglietti, J. S., Chambers, D. P., Willis, J. K., & Hilburn, K. Satellite-
490 based global-ocean mass balance estimates of interannual variability and emerging
491 trends in continental freshwater discharge. *Proceedings of the National Academy of*
492 *Sciences* **107**, 17916-17921, doi:10.1073/pnas.1003292107 (2010).
- 493 13. Rodell, M. *et al.* The observed state of the water cycle in the early 21st century. *J.*
494 *Climate* **28**, 8289-8318, doi:10.1175/JCLI-D-14-00555.1 (2015).
- 495 14. Famiglietti, J. S. *et al.* Satellites provide the big picture. *Science* **349**, 684-685,
496 doi:10.1126/science.aac9238 (2015).
- 497 15. Tapley, B. D., Bettadpur, S., Ries, J. C., Thompson, P. F., & Watkins, M. M. GRACE
498 measurements of mass variability in the Earth system. *Science* **305**, 503-505,
499 doi:10.1126/science.1099192 (2004).
- 500 16. Wahr, J., Molenaar, M., & Bryan, F. Time variability of the Earth's gravity field:
501 Hydrological and oceanic effects and their possible detection using GRACE.
502 *J. Geophys. Res. Solid Earth*, **103**, 30205-30229, doi:10.1029/98JB02844 (1998).
- 503 17. Rodell, M., & Famiglietti, J. S. Detectability of variations in continental water storage
504 from satellite observations of the time dependent gravity field. *Water Resources Res.*,
505 **35**, 2705-2723, doi:10.1029/1999WR900141 (1999).
- 506 18. Swenson, S., Yeh, P. J. F., Wahr, J., & Famiglietti, J. A comparison of terrestrial
507 water storage variations from GRACE with in situ measurements from Illinois.
508 *Geophys. Res. Lett.* **33**, L16401, doi: 10.1029/2006GL026962 (2006).
- 509 19. Cazenave, A., & Chen, J. Time-variable gravity from space and present-day mass
510 redistribution in the Earth system. *Earth and Planetary Science Letters*, **298**, 263-274,
511 doi:10.1016/j.epsl.2010.07.035 (2010).

- 512 20. Rowlands, D. D. *et al.* Resolving mass flux at high spatial and temporal resolution
513 using GRACE intersatellite measurements. *Geophys. Res. Lett.*, **32**, L04310,
514 doi:10.1029/2004GL021908 (2005).
- 515 21. Watkins, M. M., Wiese, D. N., Yuan, D. N., Boening, C. & Landerer, F. W. Improved
516 methods for observing Earth's time variable mass distribution with GRACE using
517 spherical cap mascons. *J. Geophys. Res. Solid Earth* **120**, 2648-2671,
518 doi:10.1002/2014JB011547 (2015).
- 519 22. Adler, R. *et al.* *The New Version 2.3 of the Global Precipitation Climatology Project*
520 *(GPCP) Monthly Analysis Product*.
521 http://eagle1.umd.edu/GPCP_ICDR/GPCP_Monthly.html (2016).
- 522 23. Salmon, J. M., Friedl, M. A., Frohking, S., Wisser, D., & Douglas, E. M. Global rain-
523 fed, irrigated, and paddy croplands: A new high resolution map derived from remote
524 sensing, crop inventories and climate data. *Int. J. Applied Earth Observation and*
525 *Geoinformation* **38**, 321-334, doi:10.1016/j.jag.2015.01.014 (2015).
- 526 24. Birkett, C., Reynolds, C., Beckley, B., & Doorn, B. From research to operations: the
527 USDA global reservoir and lake monitor. In *Coastal altimetry* (eds Vignudelli, S.,
528 Kostianoy, A. G., Cipollini, P., & Benveniste, J.) 19-50 (Springer, 2011).
- 529 25. IPCC Annex I: *Atlas of Global and Regional Climate Projections* (eds van
530 Oldenborgh, G. J. *et al.*) in *Climate Change 2013: The Physical Science Basis*. (eds
531 Stocker, T. F. *et al.*) 1311-1394 (IPCC, Cambridge Univ. Press, 2013).
- 532 26. Tamisiea, M. E., Leuliette, E. W., Davis, J. L., & Mitrovica, J. X. Constraining
533 hydrological and cryospheric mass flux in southeastern Alaska using space - based
534 gravity measurements. *Geophys. Res. Lett.*, **32**, L20501, doi:10.1029/2005GL023961
535 (2005).
- 536 27. Gardner, A. S. *et al.*. Sharply increased mass loss from glaciers and ice caps in the
537 Canadian Arctic Archipelago. *Nature* **473**, 357-360, doi:10.1038/nature10089
538 (2011).
- 539 28. Boening, C., Lebrock M., Landerer F., & Stephens G. Snowfall-driven mass change
540 on the East Antarctic ice sheet. *Geophys. Res. Lett.* **39**, L21501,
541 doi:10.1029/2012GL053316 (2012).
- 542 29. Schlegel, N.-J. *et al.* Application of GRACE to the assessment of model-based
543 estimates of monthly Greenland Ice Sheet mass balance (2003-2012). *The*
544 *Cryosphere*, **10**, 1965-1989, doi:10.5194/tc-10-1965-2016 (2016).
- 545 30. MacGregor, J. A. *et al.* Holocene deceleration of the Greenland Ice Sheet. *Science*
546 **351**, 590-593, doi:10.1126/science.aab1702 (2016).
- 547 31. Reager, J.T. *et al.* A decade of sea level rise slowed by climate-driven hydrology.
548 *Science* **351**, 699-703, doi:10.1126/science.aad8386 (2016).
- 549 32. Landerer, F. W., Dickey, J. O., & Güntner, A. Terrestrial water budget of the
550 Eurasian pan-Arctic from GRACE satellite measurements during 2003-2009. *J.*
551 *Geophys. Res. Atmospheres* **115**, D23, doi:10.1029/2010JD014584 (2010).
- 552 33. Famiglietti, J. S. The global groundwater crisis. *Nature Climate Change*, **4**, 945-948,
553 doi:10.1038/nclimate2425 (2014).
- 554 34. Gleeson, T., Wada, Y., Bierkens, M. F., & van Beek, L. P. Water balance of global
555 aquifers revealed by groundwater footprint. *Nature* **488**, 197-200,
556 doi:10.1038/nature11295 (2012).

- 557 35. Richey, A. S. *et al* Uncertainty in global groundwater storage estimates in a total
558 groundwater stress framework. *Water Resour. Res.*, **51**, 5198-5216,
559 doi:10.1002/2015WR017351 (2015).
- 560 36. Döll, P., Schmied, H. M., Schuh, C., Portmann, F. T., & Eicker, A. Global-scale
561 assessment of groundwater depletion and related groundwater abstractions:
562 Combining hydrological modeling with information from well observations and
563 GRACE satellites. *Water Resour. Res.* **50**, 5698-5720, doi:10.1002/2014WR015595
564 (2014).
- 565 37. Long, D. *et al*. Global analysis of spatiotemporal variability in merged total water
566 storage changes using multiple GRACE products and global hydrological models.
567 *Remote Sensing of Environment* **192**, 198-216, doi:10.1016/j.rse.2017.02.011 (2017).
- 568 38. Dalin, C., Wada, Y., Kastner, T., & Puma, M. J. Groundwater depletion embedded in
569 international food trade. *Nature* **543**, 700-704, doi:10.1038/nature21403 (2017).
- 570 39. Phillips, T., Nerem R., Fox-Kemper B., Famiglietti J., & Rajagopalan B. The
571 influence of ENSO on global terrestrial water storage using GRACE, *Geophys. Res.*
572 *Lett.* **39**, L16705, doi:10.1029/2012GL052495 (2012).
- 573 40. Humphrey, V., Gudmundsson, L., & Seneviratne, S. I. Assessing global water storage
574 variability from GRACE: Trends, seasonal cycle, subseasonal anomalies and
575 extremes. *Surveys in Geophysics* **37**, 357-395, doi:10.1007/s10712-016-9367-1
576 (2016).
- 577 41. Rodell, M., Velicogna, I., & Famiglietti, J. S. Satellite-based estimates of
578 groundwater depletion in India. *Nature* **460**, 999-1002, doi:10.1038/nature08238
579 (2009).
- 580 42. Tiwari, V. M., Wahr, J., & Swenson, S. Dwindling groundwater resources in northern
581 India, from satellite gravity observations. *Geophys. Res. Lett.* **36**, L18401,
582 doi:10.1029/2009GL039401 (2009).
- 583 43. Panda, D. K. & Wahr, J. Spatiotemporal evolution of water storage changes in India
584 from the updated GRACE-derived gravity records. *Water Resour. Res.* **52**, 135-149,
585 doi:10.1002/2015WR017797 (2016).
- 586 44. Zarfl, C., Lumsdon, A. E., Berlekamp, J., Tydecks, L., & Tockner, K. A global boom
587 in hydropower dam construction. *Aquatic Sciences* **77**, 161-170, doi:10.1007/s00027-
588 014-0377-0 (2015).
- 589 45. Wang, X., de Linage, C., Famiglietti, J., & Zender, C. S. Gravity Recovery and
590 Climate Experiment (GRACE) detection of water storage changes in the Three
591 Gorges Reservoir of China and comparison with in situ measurements. *Water Resour.*
592 *Res.* **47**, W12502, doi:10.1029/2011WR010534 (2011).
- 593 46. Chao, B. F., Wu, Y. H., & Li, Y. S. Impact of artificial reservoir water impoundment
594 on global sea level. *Science*, **320**, 212-214, doi:10.1126/science.1154580 (2008).
- 595 47. Zhang, G., Xie, H., Kang, S., Yi, D., & Ackley, S.F. Monitoring lake level changes
596 on the Tibetan Plateau using ICESat altimetry data (2003-2009). *Remote Sensing of*
597 *Environment* **115**, 1733-1742, doi:10.1016/j.rse.2011.03.005 (2011).
- 598 48. Zhang, T. Y. & Jin, S. G. Estimate of glacial isostatic adjustment uplift rate in the
599 Tibetan Plateau from GRACE and GIA models. *J. Geodynamics*, **72**, 59-66,
600 doi:10.1016/j.jog.2013.05.002 (2013).
- 601 49. Jacob, T., Wahr, J., Pfeffer, W. T., & Swenson, S. Recent contributions of glaciers
602 and ice caps to sea level rise. *Nature* **482**, 514-518, doi:10.1038/nature10847 (2012).

- 603 50. Guo, M., Wu, W., Zhou, X., Chen, Y. & Li, J. Investigation of the dramatic changes
604 in lake level of the Bosten Lake in northwestern China. *Theor. Appl. Climatol.* **119**,
605 341-351, doi:10.1007/s00704-014-1126-y (2015).
- 606 51. Stone, R. For China and Kazakhstan, no meeting of the minds on water. *Science* **337**,
607 405-407, doi:10.1126/science.337.6093.405 (2012).
- 608 52. Hao, Y., Zhu, Y., Zhao, Y., Wang, W., Du, X. & Yeh T.C.J. The role of climate and
609 human influences in the dry-up of the Jinci Springs, China. *J. Am. Water Resour.*
610 *Assoc.* **45**, 1228-1237, doi:10.1111/j.1752-1688.2009.00356.x (2009).
- 611 53. Shamsudduha, M., Taylor, R. G., & Longuevergne, L. Monitoring groundwater
612 storage changes in the highly seasonal humid tropics: Validation of GRACE
613 measurements in the Bengal Basin. *Water Resour. Res.* **48**, W02508,
614 doi:10.1029/2011WR010993 (2012).
- 615 54. Voss, K. A. *et al.* Groundwater depletion in the Middle East from GRACE with
616 implications for transboundary water management in the Tigris-Euphrates-Western
617 Iran region. *Water Resour. Res.* **49**, 904-914, doi:10.1002/wrcr.20078 (2013).
- 618 55. Sultan, M., Ahmed, M., Wahr, J., Yan, E., & Emil, M. in *Remote Sensing of the*
619 *Terrestrial Water Cycle* (eds Lakshmi, V. *et al.*), 349-366 (John Wiley & Sons, Inc,
620 Hoboken, NJ. 2014).
- 621 56. Joodaki, G., Wahr, J., & Swenson, S. Estimating the human contribution to
622 groundwater depletion in the Middle East, from GRACE data, land surface models,
623 and well observations. *Water Resour. Res.* **50**, 2679-2692,
624 doi:10.1002/2013WR014633 (2014).
- 625 57. USDA Foreign Agricultural Service. *Saudi Arabia Grain and Feed Annual, Global*
626 *Agricultural Information Network Report number SA1602*,
627 [http://gain.fas.usda.gov/Recent%20GAIN%20Publications/Grain%20and%20Feed%20](http://gain.fas.usda.gov/Recent%20GAIN%20Publications/Grain%20and%20Feed%20Annual%20Riyadh%20Saudi%20Arabia%203-14-2016.pdf)
628 [Annual Riyadh Saudi%20Arabia 3-14-2016.pdf](http://gain.fas.usda.gov/Recent%20GAIN%20Publications/Grain%20and%20Feed%20Annual%20Riyadh%20Saudi%20Arabia%203-14-2016.pdf) (2016).
- 629 58. Becker, R. H. The stalled recovery of the Iraqi marshes. *Remote Sensing* **6**, 1260-
630 1274, doi:10.3390/rs6021260 (2014).
- 631 59. Chao, N., Luo, Z., Wang, Z., & Jin, T. Retrieving Groundwater Depletion and
632 Drought in the Tigris - Euphrates Basin Between 2003 and 2015. *Groundwater*,
633 doi:10.1111/gwat.12611 (2017).
- 634 60. Zmijewski, K., & Becker, R. Estimating the effects of anthropogenic modification on
635 water balance in the Aral Sea watershed using GRACE: 2003–12. *Earth Interactions*
636 **18**, 1-16, doi:10.1175/2013EI000537.1 (2014).
- 637 61. Chen, J.L., Pekker, T., Wilson, C.R., Tapley, B.D., Kostianoy, A.G., Cretaux, J.-F., &
638 Safarov, E.S. Long-term Caspian Sea level change. *Geophys. Res. Lett.* **44**, 6993–
639 7001, doi:10.1002/2017GL073958 (2017).
- 640 62. Han, S.-C., Sauber, J., Luthcke, S. B., Ji, C., & Pollitz, S. S. Implications of
641 postseismic gravity change following the great 2004 Sumatra-Andaman earthquake
642 from the regional harmonic analysis of GRACE intersatellite tracking data. *J.*
643 *Geophys. Res. Solid Earth* **113**, B11413, doi:10.1029/2008JB005705 (2008).
- 644 63. Han, S. C., Sauber, J., & Riva, R. Contribution of satellite gravimetry to
645 understanding seismic source processes of the 2011 Tohoku-Oki earthquake.
646 *Geophys. Res. Lett.* **38**, L24312, doi:10.1029/2011GL049975 (2011).

- 647 64. Peltier, W.R., Argus, D. F., & Drummond, R. Space geodesy constrains ice age
648 terminal deglaciation: The global ICE-6G_C (VM5a) model. *J. Geophys. Res. Solid*
649 *Earth* **120**, 450–487, doi:10.1002/2014JB011176 (2015).
- 650 65. Peltier, W.R., Argus, D. F. & Drummond, R. Comment on the paper by Purcell et al
651 (2016) entitled “An Assessment of the ICE-6G_C (VM5a) glacial isostatic adjustment
652 model. *J. Geophys. Res. Solid Earth* **122** , doi:10.1002/2016JB013844 (2017).
- 653 66. Forman, B. A., Reichle, R. H., & Rodell, M., Assimilation of terrestrial water storage
654 from GRACE in a snow-dominated basin. *Water Resour. Res* **48**, W01507,
655 doi:10.1029/2011WR011239 (2012).
- 656 67. Bouchard, F. *et al.* Vulnerability of shallow subarctic lakes to evaporate and desiccate
657 when snowmelt runoff is low. *Geophys. Res. Lett.* **40**, 6112–6117,
658 doi:10.1002/2013GL058635 (2013).
- 659 68. Reager, J. T. *et al.* Assimilation of GRACE terrestrial water storage observations into
660 a land surface model for the assessment of regional flood potential. *Remote Sensing* **7**,
661 14663-14679, doi:10.3390/rs71114663 (2015).
- 662 69. Famiglietti, J.S. *et al.* Satellites measure recent rates of groundwater depletion in
663 California's Central Valley. *Geophys. Res. Lett.* **38**, L03403,
664 doi:10.1029/2010GL046442 (2011).
- 665 70. Scanlon, B.R., et al. Groundwater depletion and sustainability of irrigation in the US
666 High Plains and Central Valley. *PNAS* **109**, 9320-9325,
667 doi:10.1073/pnas.1200311109 (2012).
- 668 71. Faunt, C. C., Sneed, M., Traum, J. & Brandt, J. T. Water availability and land
669 subsidence in the Central Valley, California, USA. *Hydrogeology Journal* **24**, 675-
670 684, doi:10.1007/s10040-015-1339-x (2016).
- 671 72. Belmecheri, S., Babst, F., Wahl, E.R., Stahle, D.W., & Trouet, V. Multi-century
672 evaluation of Sierra Nevada snowpack. *Nature Climate Change*, **6**, 2-3,
673 doi:10.1038/nclimate2809 (2016).
- 674 73. Fernando, D. N. *et al.* What caused the spring intensification and winter demise of the
675 2011 drought over Texas?. *Climate Dynamics* **47**, 3077-3090, doi:10.1007/s00382-
676 016-3014-x (2016).
- 677 74. Haacker, E. M., Kendall, A. D., & Hyndman, D. W. Water level declines in the high
678 plains aquifer: Predevelopment to resource senescence. *Groundwater* **54**, 231-242,
679 doi:10.1111/gwat.12350 (2016).
- 680 75. Willis, M. J., Melkonian, A. K., Pritchard, M. E., & Ramage, J. M. Ice loss rates at
681 the Northern Patagonian Icefield derived using a decade of satellite remote sensing.
682 *Remote Sensing of Environment* **117**, 184-198, doi:10.1016/j.rse.2011.09.017 (2012).
- 683 76. Chen, J. L., Wilson, C. R., Tapley, B. D., Blankenship, D. D., & Ivins, E. R.
684 Patagonia icefield melting observed by gravity recovery and climate experiment
685 (GRACE). *Geophys. Res. Lett.* **34**, L22501, doi:10.1029/2007GL031871 (2007).
- 686 77. Han, S. C., Sauber, J., & Luthcke, S. Regional gravity decrease after the 2010 Maule
687 (Chile) earthquake indicates large-scale mass redistribution. *Geophys. Res. Lett.* **37**,
688 L23307, doi:10.1029/2010GL045449 (2010).
- 689 78. Chen, J. L., Wilson, C. R., & Tapley, B. D. The 2009 exceptional Amazon flood and
690 interannual terrestrial water storage change observed by GRACE. *Water Resour Res.*
691 **46**, W12526, doi:10.1029/2010WR009383 (2010).

- 692 79. Thomas, A. C., Reager, J. T., Famiglietti, J. S., & Rodell, M. A GRACE-based water
693 storage deficit approach for hydrological drought characterization. *Geophys. Res.*
694 *Lett.* **41**, 1537-1545, doi:10.1002/2014GL059323 (2014).
- 695 80. Getirana, A. C. Extreme water deficit in Brazil detected from space. *J.*
696 *Hydrometeorol.* **17**, 591-599, doi:10.1175/JHM-D-15-0096.1 (2015).
- 697 81. Gaughan, A. E. & Waylen, P. R. Spatial and temporal precipitation variability in the
698 Okavango–Kwando–Zambezi catchment, southern Africa. *J. Arid Environments* **82**,
699 19-30, doi:10.1016/j.jaridenv.2012.02.007 (2012).
- 700 82. Andersen, O. B., et al. Terrestrial water storage from GRACE and satellite altimetry
701 in the Okavango Delta (Botswana). *Gravity, Geoid and Earth Observation,*
702 *International Association of Geodesy Symposia* Vol. **135** (ed. Mertikas, S.) 521-526
703 (Springer, 2010).
- 704 83. Swenson, S., & Wahr, J. Monitoring the water balance of Lake Victoria, East Africa,
705 from space. *J. Hydrology* **370**, 163-176, doi:10.1016/j.jhydrol.2009.03.008 (2009).
- 706 84. Ahmed, M., Sultan, M., Wahr, J., & Yan, E. The use of GRACE data to monitor
707 natural and anthropogenic induced variations in water availability across Africa.
708 *Earth-Sci. Rev.* **136**, 289-300, doi:10.1016/j.earscirev.2014.05.009 (2014).
- 709 85. Ndehedehe, C. E., Awange, J. L., Kuhn, M., Agutu, N. O., & Fukuda Y. Climate
710 teleconnections influence on West Africa's terrestrial water storage. *Hydrological*
711 *Proc.* **31**, 3206–3224, doi:10.1002/hyp.11237 (2017).
- 712 86. Crowley, J. W., Mitrovica, J. X., Bailey, R. C., Tamisiea, M. E., & Davis, J. L. Land
713 water storage within the Congo Basin inferred from GRACE satellite gravity data.
714 *Geophys. Res. Lett.* **33**, L19402, doi:10.1029/2006GL027070 (2006).
- 715 87. Ramillien, G., Frappart, F., & Seoane, L. Application of the regional water mass
716 variations from GRACE satellite gravimetry to large-scale water management in
717 Africa. *Remote Sensing* **6**, 7379-7405, doi:10.3390/rs6087379 (2014).
- 718 88. Van Dijk, A. *et al.* The Millennium Drought in southeast Australia (2001–2009):
719 Natural and human causes and implications for water resources, ecosystems,
720 economy, and society. *Water Resources Res.* **49**, 1040-1057, doi:10.1002/wrcr.20123
721 (2013).
- 722 89. Boening, C., Willis, J. K., Landerer, F. W., Nerem, R. S., & Fasullo, J. The 2011 La
723 Niña: So strong, the oceans fell. *Geophys. Res. Lett.* **39**, L19602,
724 doi:10.1029/2012GL053055 (2012).
- 725 90. Munier, S., Becker, M., Maisongrande, P., & Cazenave A. Using GRACE to detect
726 Groundwater Storage variations: the cases of Canning Basin and Guarani aquifer
727 system. *Int. Water Tech. J.* **2**, 2–13 (2012).
- 728 91. Jaramillo, F., & Destouni, G. Local flow regulation and irrigation raise global human
729 water consumption and footprint. *Science* **350**, 1248-1251,
730 doi:10.1126/science.aad1010 (2015).
- 731 92. Fietelson, E. The four Eras of Israeli water policy. *Water policy in Israel: Context,*
732 *Issues and Options* (ed. Becker, N.) 15-32 (Springer, 2013).
- 733 93. Bhanja, S. N. *et al.* Groundwater rejuvenation in parts of India influenced by water-
734 policy change implementation. *Scientific Reports* **7**, 7453, doi:10.1038/s41598-017-
735 07058-2 (2017).

- 736 94. Eicker, A., Forootan, E., Springer, A., Longuevergne, L., & Kusche, J. Does GRACE
737 see the terrestrial water cycle “intensifying”? *J. Geophys. Res. Atmos.* **121**, 733-745,
738 doi:10.1002/2015JD023808 (2016).
- 739 95. Kusche, J., Eicker, A., Forootan, E., Springer, A., & Longuevergne, L. Mapping
740 probabilities of extreme continental water storage changes from space gravimetry.
741 *Geophys. Res. Lett.* **43**, 8026-8034, doi:10.1002/2016GL069538 (2016).
- 742 96. Green, T. R. *et al.* Beneath the surface of global change: Impacts of climate change
743 on groundwater. *J. Hydrology* **405**, 532-560, doi:10.1016/j.jhydrol.2011.05.002
744 (2011).
- 745 97. Taylor, R. G. *et al.* Ground water and climate change. *Nature Climate Change* **3**, 322-
746 329, doi:10.1038/nclimate1744 (2013).
- 747 98. Swenson, S. C., & Milly, P. C. D. Climate model biases in seasonality of continental
748 water storage revealed by satellite gravimetry. *Water Resour. Res.* **42**, W03201,
749 doi:10.1029/2005WR004628 (2006).
- 750 99. McCabe, M. F. *et al.* The future of Earth observation in hydrology. *Hydrology and*
751 *Earth System Science* **21**, 3879–3914, doi:10.5194/hess-21-3879-2017 (2017).
- 752 100. Flechtner, F. *et al.* What can be expected from the GRACE-FO Laser Ranging
753 Interferometer for Earth Science applications? *Surveys in Geophysics* **37**, 453-470,
754 doi:10.1007/s10712-015-9338-y (2016).

755
756
757

Acknowledgements

758 We thank the German Space Operations Center of the German Aerospace Center (DLR)
759 for providing continuously and nearly 100% of the raw telemetry data of the twin GRACE
760 satellites. Landsat is an interagency program managed by NASA and the U.S. Geological
761 Survey. Lake products courtesy of the USDA/NASA G-REALM program at
762 http://www.pecad.fas.usda.gov/cropexplorer/global_reservoir/. Valentina Khan of the
763 Hydrometeorological Research Center of the Russian Federation assisted with the Volga
764 River discharge analysis. Graphics were produced by Amy K. Moran, Global Science &
765 Technology, Inc. This research was funded by NASA’s GRACE Science Team and
766 NASA’s Energy and Water Cycle Study (NEWS) Team; the University of California
767 Office of the President, Multicampus Research Programs and Initiatives; the NASA Earth
768 and Space Science Fellowship program; the Jet Propulsion Laboratory; and the Ministry of
769 Science and Technology, Taiwan. Portions of this research were conducted at the Jet

770 Propulsion Laboratory, which is operated for NASA under contract with the California
771 Institute of Technology. We also thank two anonymous reviewers for helping to improve
772 the quality of the manuscript.

773

774 **Author Contributions**

775 M.R. and J.S.F. performed background research and designed the study with input from
776 J.T.R. and M.-H.L. D.N.W. and J.T.R. led the GRACE data and error analysis with
777 assistance from F.W.L. M.R. and F.W.L. designed the figures with additional data
778 prepared by H.K.B. M.R. and J.S.F. wrote the manuscript. All authors discussed the
779 results and commented on the manuscript.

780

781 **Author Information**

782 Reprints and permissions information are available at www.nature.com/reprints. The
783 authors claim no competing financial interests. Correspondence and requests for materials
784 should be addressed to Matthew.Rodell@nasa.gov.

785

786

787 **Tables**

788

Region #	Location	Area (km ²)	TWS Trend (Gt/yr)	TWS Trend Errors (Gt/yr)	r ² of TWS Trend (-)	Irrigated Area (%)	Precipitation Trend (mm/yr)	Precipitation Trend (%/yr)	Precipitation Percentage of Normal (%)	Predicted Precipitation Change (%)
1	Antarctica	12,397,401	-127.6	39.9	0.93	0	0.82	0.40	96.6	30.9
2	Greenland	2,184,307	-279.0	23.2	0.97	0	8.85	2.09	102.7	39.1
3	Gulf Coast of Alaska	716,492	-62.6	8.2	0.93	0	-3.03	-0.25	95.0	21.3
4	Canadian Archipelago	672,413	-74.6	4.1	0.95	0	-5.33	-2.11	94.5	38.3
5	N North America	1,350,129	6.1	5.8	0.52	0	2.35	0.73	105.1	26.9
6	N Eurasia	8,009,175	13.4	9.7	0.10	0	1.65	0.30	104.4	25.1
7	N India	664,169	-19.2	1.1	0.80	54	15.80	2.20	101.0	11.8
8	Central India	1,352,670	9.4	0.6	0.24	51	3.72	0.36	103.7	23.1
9	E Central China	657,375	7.8	1.6	0.78	14	7.33	0.77	99.6	7.9
10	Tibetan Plateau	881,704	7.7	1.4	0.67	0	-1.52	-0.90	104.2	19.7
11	NW China	215,152	-5.5	0.5	0.77	7	1.11	0.57	109.8	15.3
12	N China Plain	876,004	-11.3	1.3	0.63	52	-2.33	-0.37	103.0	19.4
13	E India Region	1,228,839	-23.3	1.9	0.85	25	-9.52	-0.67	96.1	14.7
14	NW Saudi Arabia	841,763	-10.5	1.5	0.92	0	-1.44	-1.31	77.7	-1.4
15	N Middle East	2,189,561	-32.1	1.5	0.84	5	-2.80	-0.90	96.3	-8.5
16	SW Russia Region	1,772,712	-18.1	1.3	0.64	15	-5.83	-0.92	96.8	6.2
17	Aral Sea	52,299	-2.2	0.1	0.76	0	2.71	1.17	111.1	5.9
18	Caspian Sea	377,761	-23.7	4.2	0.76	0	-4.37	-1.14	103.4	2.1
19	Central Canada	802,682	-7.0	6.4	0.73	0	0.69	0.17	102.0	16.9
20	N Great Plains	1,333,598	20.2	4.8	0.79	3	2.26	0.44	102.0	7.0
21	S California	177,996	-4.2	0.4	0.46	18	-8.31	-1.29	89.7	1.2
22	S High Plains and E Texas	1,105,113	-12.2	3.6	0.44	9	-5.71	-0.76	95.2	-2.8
23	Patagonian Ice Fields	461,198	-25.7	5.1	0.89	0	-8.01	-0.76	97.1	-6.9
24	Central Argentina*	530,661	-8.6	1.2	0.77	4	1.87	0.32	94.2	0.7
25	Central & W Brazil	5,559,805	51.9	9.4	0.39	1	0.61	0.03	100.2	-5.0
26	E Brazil	1,132,450	-16.7	2.9	0.39	1	-16.97	-1.61	97.7	-5.9
27	Okavango Delta	1,589,692	29.5	3.5	0.55	0	-5.21	-0.61	105.3	-8.7
28	Nile Headwaters	1,824,276	21.9	3.9	0.56	1	-3.53	-0.30	97.7	11.6
29	Tropical W Africa	2,298,134	24.1	2.1	0.67	1	-0.12	-0.01	103.4	-6.3
30	N Congo	1,318,261	-7.2	1.0	0.26	0	-1.55	-0.10	99.1	7.1
31	SE Africa	1,677,719	-12.9	2.3	0.47	0	-3.23	-0.32	95.9	-5.9
32	N Africa	6,664,135	-11.7	2.9	0.45	1	-0.12	-0.19	106.7	-12.9
33	N & E Australia	2,504,494	19.0	2.8	0.32	3	4.30	0.69	104.6	-6.0
34	NW Australia	1,002,367	-8.9	1.2	0.43	0	-0.39	-0.10	99.1	-0.6

Table 1. TWS trends and supporting information. Location, area, GRACE terrestrial water storage trend (April 2002 – March 2016) and uncertainty, coefficient of determination (r^2) of the fitted linear trend, percentage of the area equipped for irrigation²³, trend in precipitation²² (January 2002 to March 2016) after removing the seasonal cycle, annual mean precipitation (2003-2015) as a percentage of the long term (1979-2015) annual mean²², and median predicted change in precipitation between 1986-2005 and 2081-2100 in the IPCC high end greenhouse gas emissions scenario²⁵ for each of the 34 study regions. *The TWS Trend in Region 24 is for April 2002 – February 2010 only.

790

791 **Figure Captions**

792 **Figure 1. Annotated map of terrestrial water storage trends.** Trends in TWS
 793 (cm/yr) based on GRACE observations from April 2002 to March 2016. The cause of
 794 the trend in each outlined study region is briefly explained and color coded by
 795 category. The trend map was smoothed with a 150 km radius Gaussian filter for the
 796 purpose of visualization, however, all calculations were performed at the native 3°
 797 resolution of the data product.

798 **Figure 2. Trends in terrestrial water storage and supporting data maps.**
 799 (Bottom to top) TWS trends (cm/yr); percentage of area equipped for irrigation²³
 800 (%); trend in precipitation²²; mean annual precipitation (2003-2015) as a percentage
 801 of the long term mean²²; IPCC predicted change in precipitation²⁵. Areas outside of
 802 the study regions are shaded.

803 **Methods**

804 GRACE data have traditionally been processed by solving for gravity anomalies in
805 terms of Stokes coefficients^{101, 102, 103, 104, 105, 106}. These solutions suffer from correlated
806 errors that manifest as longitudinal striping in the gravity solution, requiring tailored
807 “destriping” and smoothing post-processing filters to remove¹⁰⁷. While largely successful
808 in removing errors, the post-processing also damps and smooths real geophysical
809 signals¹⁰¹. Recent advances in GRACE data processing have shown that solving for gravity
810 anomalies in terms of mass concentration (‘mascon’) functions with carefully selected
811 regularization results in superior localization of signals on an elliptical Earth^{4, 21, 108, 109}.
812 For instance, mascon solutions correlate better with in-situ ocean bottom pressure recorders
813 than spherical harmonic solutions^{21, 109}, improve the spatial resolution of mass changes in
814 Greenland²⁹, and were used to detect changes in the Atlantic Meridional Overturning
815 Circulation¹¹⁰. Currently, there are three publicly available GRACE mascon solutions: Jet
816 Propulsion Laboratory mascons RL05M.1 version 2^{21, 111} (JPL-M), Center for Space
817 Research mascons RL05M¹⁰⁹ (CSR-M), and Goddard Space Flight Center mascons version
818 2.3b⁴ (GSFC-M). JPL-M parameterizes the gravity field with 4,551 equal-area 3° mascon
819 elements, while CSR-M and GSFC-M both parameterize the gravity field in terms of 1°
820 mascon elements (~41,000 mascon elements are solved for in each solution). The
821 implementation details of each mascon solution differs, but we note that the JPL solution
822 has the unique characteristic that each 3° mascon element is relatively uncorrelated with
823 neighboring mascon elements, while the 1° mascon elements in the CSR and GSFC are
824 highly correlated with their neighbors. Three degrees corresponds approximately to the
825 ‘native’ resolution of GRACE, and being uncorrelated with one another in the retrieval

826 allows for a quantitative understanding of leakage errors when aggregating mass anomalies
827 within a hydrological basin¹¹²; in fact, no literature yet exists on quantifying leakage errors
828 in 1° mascon solutions. As such, in this manuscript, we use the JPL RL05M GRACE
829 mascon solution for trend analysis and mapping; however, we use all (i.e., JPL-M, CSR-
830 M, and GSFC-M) mascon solutions to derive uncertainties.

831 The JPL RL05M GRACE mascon solution parameterizes each monthly gravity field in
832 terms of 4,551 equal-area surface spherical cap mass concentration functions, and uses a
833 regularization approach that implements both spatial and temporal correlations to remove
834 correlated errors during the gravity inversion. A Coastline Resolution Improvement (CRI)
835 filter is used to separate between land and ocean mass within mascons that span
836 coastlines¹¹². GRACE does not produce a reliable estimate of the Earth's oblateness (C_{20}
837 coefficient), and as such, we follow the standard protocol of using Satellite Laser Ranging
838 to provide this estimate¹¹³. Further, GRACE gravity field anomalies are measured in the
839 center of mass Earth reference frame, and therefore need to be augmented with a
840 'geocenter' estimate to capture all surface mass changes¹¹⁴. GIA corrections are made
841 using the updated ICE-6G_D model^{64, 65}, with an exception for Antarctica, for which we
842 reduce the fitted rate of mass change by 9.2 Gt/yr based on a regional model¹¹⁵ that
843 potentially provides a better GIA estimate for Antarctica¹¹⁶. Finally, corrections are made
844 to the C_{21} and S_{21} coefficients¹¹⁷ in order to fully remove the pole tide from the GRACE
845 data. Jumps in the background atmosphere and ocean dealiasing product are corrected as
846 well¹¹⁸.

847 Prior to computing the best fit linear trend from a TWS time series, the seasonal cycle
848 was removed as follows. First, missing months of data were filled by linear interpolation.

849 Next, the mean monthly seasonal cycle was computed by averaging all Januarys, all
850 Februarys, etc. Finally, for each month in the original, non-gap-filled time series, the mean
851 for the corresponding month of the year was subtracted. The first step, gap filling, was
852 necessary because, for example, the month of May was under-sampled in the second half
853 of the study period, which caused the mean May to be biased in locations where a consistent
854 trend existed (i.e., most of the regions of this study).

855 Trend error estimates account for both systematic and random GRACE measurement
856 errors as well as systematic GIA model error. GRACE measurement error is taken to be
857 the 1-sigma standard deviation between trend estimates obtained from JPL-M, CSR-M,
858 and GSFC-M. Given the specific basin boundaries used in this study, we find JPL-M to
859 have more pronounced trends (both positive and negative) than CSR-M and GSFC-M,
860 which is consistent with previous conclusions¹¹⁹. This spread is due to a fundamental
861 difference in the spectral content between the 3° mascons and 1° mascons, implying that
862 leakage characteristics are different when aggregating mass anomalies over a particular
863 region (somewhat counter-intuitively, the 3° mascons ‘focus’ more signal than the 1°
864 sampled mascons). In essence, the ‘smooth’ nature of the 1° mascon solutions (CSR-M
865 and GSFC-M) results in significant damping of signal over our regions of interest due to
866 leakage across the basin boundaries. For a more direct comparison of the three solutions
867 over our regions of interest, we matched the spectral content of JPL-M to that of CSR-M.
868 The regularization of the CSR mascon solution is based on a 200 km Gaussian smoothed
869 representation of a regularized spherical harmonic solution¹⁰⁹; hence, it is expected that the
870 final mascon solution will inherit some of these spectral characteristics. Thus, we smooth
871 JPL-M with a Gaussian filter with a 200 km radius, and compare trend estimates of the

872 smoothed version of JPL-M to CSR-M and GSFC-M. The agreement is now significantly
873 better, and trends in the smoothed version of JPL-M are now also damped similarly to
874 CSR-M and GSFC-M (see Figure ED9 for an example). Analog analysis has been
875 performed before by others in studying mass variations over the Caspian Sea¹²⁰. We use
876 the 1-sigma standard deviation of trend estimates obtained from the smoothed version of
877 JPL-M, CSR-M, and GSFC-M to derive the GRACE measurement errors. GIA model
878 error is taken to be the 1-sigma spread between four competing GIA models^{64, 65, 121, 122, 123,}
879 ¹²⁴ that implement two distinct loading histories, four distinct viscosity profiles, and
880 different implementation of physics. The uncertainty on the trend for any region is given
881 by the root sum of squares combining the GIA model error (which only manifests as a
882 trend) and the GRACE measurement error.

883 Time series for the Aral and Caspian Seas (regions 17 and 18) were calculated by
884 applying a set of gain factors to the GRACE data. Gain factors act to redistribute mass
885 within each individual mascon (at sub-mascon resolution), allowing for exact averaging
886 kernels to be applied to a region of interest and retrieval of accurate, unbiased (by leakage)
887 mass change values^{112,125}. These particular gain factors were derived¹¹² via a combination
888 of total column soil moisture output from the Noah land surface model driven by the Global
889 Land Data Assimilation System¹⁰⁰ (which does not include sea water variations) along with
890 altimetry data¹²⁷ over the Seas.

891 Recent variations in Caspian Sea Level have been attributed by previous studies to
892 natural meteorological variability⁸ and direct evaporation from the sea surface⁶¹. We tested
893 these two theories and a third, agricultural water consumption. Flow in the Volga River,
894 which delivers roughly 80% of the runoff to the Caspian Sea, is controlled by a series of

895 eleven dams¹²⁸. Among other purposes these ensure a steady supply of water for crop
896 irrigation¹²⁸. Data to quantify interannual variations in irrigation extent, intensity, or
897 volumes in the Caspian Sea drainage basin during the study period were not available.
898 Estimates of Russian wheat, maize, rice, and soybean annual production¹²⁹ (in tons) during
899 1992-2015 were obtained from the Organisation for Economic Co-operation and
900 Development (OECD). According to the irrigation dataset²³, the Volga River basin, which
901 drains to the Caspian Sea, includes 3% irrigated crops and 37% rain-fed crops by area, and
902 it accounts for about half of all Russian crop production, so the latter is a fair but imperfect
903 indicator of agricultural water demand in the basin. Yearly total production was
904 normalized by subtracting the 24-year mean and dividing by the standard deviation.
905 Normalization was similarly performed on annual time series of GPCP precipitation²² over
906 the Caspian Sea and Volga River drainage basins, Volga River discharge, reanalysis based
907 Caspian Sea evaporation¹³⁰, and changes in Caspian Sea level from satellite altimetry²⁴.
908 Correlation coefficients (and significance levels) between normalized Caspian Sea level
909 change and its significant drivers (Figure ED10) were 0.78 (Volga River discharge;
910 $p < 0.001$), -0.47 (crop production; $p = 0.02$), -0.43 (Caspian Sea evaporation; $p = 0.04$), and
911 0.41 (Caspian Sea drainage basin precipitation; $p = 0.05$). Correlation coefficients (and
912 significance levels) between normalized Volga River discharge and significant drivers
913 were 0.52 (Volga River basin precipitation; $p = 0.01$) and -0.40 (crop production; $p = 0.06$).
914 Notably, the correlation between crop production and precipitation was negligible,
915 suggesting that irrigation effectively mitigates the impact of drought. Interannual
916 variations in Caspian Sea evaporation do, indeed, contribute significantly to Caspian Sea
917 level changes. However, annual Volga River discharge variations are better correlated with

918 annual changes in Caspian Sea level, they are larger than variations in Caspian Sea
919 evaporation (standard deviation of 48 Gt vs. 18 Gt, compared with 38 Gt mean magnitude
920 of annual Caspian Sea level change), and they are controlled by both precipitation and
921 rising agricultural water demand¹²⁸. We therefore conclude that all three factors
922 contributed to the observed water loss (-23.7 ± 4.2 Gt/yr based on GRACE, ignoring steric
923 effects; -25.4 Gt/yr based on satellite altimetry) during 2002-2015.

924 For the Gulf Coast of Alaska and Patagonian Ice Fields (regions 3 and 23) it was also
925 necessary to increase the rates of mass loss (by 7 Gt/yr and 9 Gt/yr, respectively) to account
926 for Little Ice Age GIA³¹. Note the full GIA corrections to Antarctica, the Gulf Coast of
927 Alaska, and the Patagonian Ice Fields are not incorporated into Figures ED1 and ED3.

928 The irrigated area percentages (Table 1) were computed by area-weighted averaging of
929 the individual pixel values of irrigation intensity²³ (%) within each study region.
930 Precipitation trends (mm/yr) were computed based on monthly data²² as above for TWS,
931 except that there were no gaps to fill. Precipitation trends (%/yr) and precipitation
932 percentages of normal were computed using the 1979-2015 annual mean precipitation
933 totals for each region. Predicted precipitation changes were computed as area weighted
934 averages from the IPCC dataset²⁵ over the study regions. The precipitation maps in Figure
935 2 were computed as above but on a pixel by pixel basis.

936 The explanation for the mass loss trend in northwest China (region 11), -5.5 ± 0.5 Gt/yr,
937 is complex. Drought was not a factor given that precipitation was 10% above normal and
938 stable during the period. Two recent studies^{131, 132} estimated the rate of glacier loss over
939 the entire Tien Shan mountain range to be -5.4 ± 2.9 Gt/yr and -7.5 ± 3.4 Gt/yr based on Ice,
940 Cloud and Land Elevation Satellite (ICESat) observations from 2003 to 2009. These

941 estimates are somewhat smaller than our GRACE based estimate of TWS decline in region
942 11 during that period (-8.3 ± 0.8 Gt/yr), despite region 11 encompassing less than half of
943 the area of glacier melt¹³¹. Thus we conjecture that an additional catalyst for mass loss
944 must exist. Xinjiang province is one of the world's largest producers of coal, having an
945 estimated 2.2 trillion tons of reserves¹³³. Reported rates of coal removal and burning
946 themselves are more than an order of magnitude smaller than the GRACE-observed mass
947 loss¹³³, but mining involves dewatering of the aquifers that the mines intersect. Consequent
948 groundwater depletion in the area is possible⁵² but unconfirmed. Adding to the complexity,
949 region 11 lies within a larger, endorheic basin, meaning that water pumped from the ground
950 or melting from glaciers will remain as surface water, become groundwater recharge,
951 and/or evapotranspire, as opposed to flowing to the ocean. However, based on satellite
952 altimetry data, the elevations of the five lakes within the surrounding endorheic basin did
953 not increase during the study period. All either declined or did not change significantly.
954 The two lowlands into which region 11 drains (one northwest, one southeast) have
955 GRACE-based trends of 0.3 and -0.6 Gt/yr (both insignificant). Ultimately
956 evapotranspiration must account for the water lost from region 11. The average annual
957 precipitation in region 11 is 194 mm/yr, making it the fourth driest of the 32 study regions.
958 The endorheic basin is extensively irrigated, including 7% of region 11, and irrigation
959 intensity is likely rising in support of Xinjiang province's population growth (18.2 million
960 to 21.8 million between 2000 and 2010)⁵¹. Massive amounts of surface water from Lake
961 Bosten and the Kongque River (both southeast of region 11) are transferred via aqueducts
962 southward to the Tarim River in order to support farming in the arid plains, yet the Tarim
963 River runs dry before reaching its natural terminus, Lop Nor lake⁵⁰. To summarize, the

964 Tien Shan mountain glaciers in region 11 are shrinking due to global warming.
965 Groundwater may be declining due to agricultural withdrawals and/or mining operations,
966 but the latter is unconfirmed. Because region 11 lies within an endorheic basin, neither
967 glacier melt nor groundwater pumping can alone explain the observed TWS depletion. The
968 corollary is that the resulting additions to surface water are balanced by desert- and
969 irrigation-enhanced evapotranspiration.

970 As noted in the main text, previous GRACE based studies of the North China Plain
971 (region 12), while agreeing that groundwater depletion associated with intense irrigation
972 was the cause, offered a wide range of estimates of the TWS or groundwater trend.
973 Specifically, put into common units, these estimates equated to -8.3 Gt/yr over a 370,000
974 km² area¹³⁴, -35 Gt/yr over a 2,086,000 km² area¹³⁵, -2.33 Gt/yr over a 370,000 km² area¹³⁶,
975 and -14.09 Gt/yr over a 1,500,000 km² area¹³⁷, compared with our estimate of -11.3 Gt/yr
976 over a 876,004 km² area.

977

978 **Data Availability**

979 Specific sources of data used in this study were the following. The primary GRACE
980 TWS dataset is JPL Mascon RL05M.1 version 2 was accessed 3 February 2017 from
981 https://grace.jpl.nasa.gov/data/get-data/jpl_global_mascons/. Additional GRACE TWS
982 datasets used to estimate errors were CSR RL05 Mascon version 1 accessed 20 September
983 2017 from http://www2.csr.utexas.edu/grace/RL05_mascons.html and GSFC Mascon
984 version 2.3b accessed 5 October 2017 from
985 <https://neptune.gsfc.nasa.gov/gngphys/index.php?section=413>. Primary GIA data used in
986 this study were the ICE-6GD model accessed 1 December 2017 from

987 <http://www.atmosph.physics.utoronto.ca/~peltier/data.php> and the IJ05_R2 GIA correction
988 for Antarctica accessed 3 February 2018 from
989 <http://onlinelibrary.wiley.com/doi/10.1002/jgrb.50208/full>. Additional GIA data used to
990 compute GIA model error included ICE-6G_ANU_D accessed 3 February 2018 from
991 <http://onlinelibrary.wiley.com/doi/10.1002/2017JB014930/full>, the A et al. (2013) GIA
992 model accessed 16 December 2013 from [ftp://podaac-](ftp://podaac-ftp.jpl.nasa.gov/allData/tellus/L3/pgr/)
993 [ftp.jpl.nasa.gov/allData/tellus/L3/pgr/](ftp://podaac-ftp.jpl.nasa.gov/allData/tellus/L3/pgr/), and the Paulson et al. (2007) GIA model accessed
994 3 February 2018 from <https://academic.oup.com/gji/article/171/2/497/2018541>.
995 Atmosphere and ocean dealiasing product jump corrections were accessed 13 June 2016
996 from <ftp://podaac-ftp.jpl.nasa.gov/allData/grace/docs/>. GPCP version 2.3 precipitation
997 data were accessed 23 September 2016 from
998 <https://www.esrl.noaa.gov/psd/data/gridded/data.gpcp.html>. Global Rain-fed Irrigation
999 and Paddy Croplands version 1 data were accessed 12 September 2016 from [http://ftp-](http://ftp-earth.bu.edu/public/friedl/GRIPCmap/)
1000 [earth.bu.edu/public/friedl/GRIPCmap/](http://ftp-earth.bu.edu/public/friedl/GRIPCmap/). Global Reservoirs/Lakes elevation version
1001 TPJO.2.3 data were accessed 29 July 2016 from
1002 https://ipad.fas.usda.gov/cropexplorer/global_reservoir/. IPCC 5th Assessment Report
1003 (RCP8.5) predicted precipitation change data were accessed 1 September 2016 from
1004 https://www.ipcc.ch/pdf/assessment-report/ar5/wg1/WG1AR5_AnnexI_FINAL.pdf.
1005 Russian crop production data were accessed 16 August 2017 from
1006 <https://data.oecd.org/agroutput/crop-production.htm>. Latent heat flux (evapotranspiration)
1007 data for the Caspian Sea and its drainage basin were extracted from MERRA2 Land
1008 Surface Diagnostics version M2TMNXLND_5.12.4, accessed 19 September 2017 from
1009 https://disc.sci.gsfc.nasa.gov/datasets/M2TMNXLND_5.12.4/summary. Volga River

1010 discharge observations are restricted from public access, but a time series of normalized
1011 annual discharge values was provided to M.R. by Valentina Khan of the
1012 Hydrometeorological Research Center of the Russian Federation.

1013 The JPL RL05M GRACE solution used in this study is identical to that which is
1014 available from the NASA/JPL GRACE Tellus website with exception that we implemented
1015 a different GIA model, a correction to the pole tide, and corrections to the background
1016 atmosphere/ocean dealiasing model. These adjustments are available from D.N.W. upon
1017 request. Data analyzed to create Figure ED9 are available from D.N.R. upon request.
1018 Excel spreadsheets containing the data and calculations used to create Table 1 and Figure
1019 ED10 are available from M.R. upon request.

1020

1021 **Code Availability**

1022 GRACE based TWS time series for the study regions were prepared, including GIA
1023 adjustments, C_{21} and S_{21} coefficient replacements, and corrections due to jumps in the
1024 atmosphere and ocean dealiasing products, using MATLAB scripts. These are available
1025 upon reasonable request from D.N.W. TWS time series analyses, including trend
1026 estimation and r^2 computation, were performed within Excel spreadsheets, which are
1027 available from M.R. upon reasonable request.

1028

1029 **Methods References**

- 1030 101. Landerer, F. W., & Swenson, S. C. (2012). Accuracy of scaled GRACE terrestrial
1031 water storage estimates. *Water Resour. Res.* **48**, W04531,
1032 doi:10.1029/2011WR011453 (2012).
1033 102. Dahle, C., et al. GFZ RL05: an improved time-series of monthly GRACE gravity
1034 field solutions. *Observation of the System Earth from Space-CHAMP, GRACE,*

- 1035 *GOCE and Future Missions* (eds. Flechtner, F., Sneeuw, N., & Schuh, W.D.) 29-39
1036 (Springer, 2014).
- 1037 103. Mayer-Gürr, T., et al. ITSG-Grace2016 - Monthly and Daily Gravity Field
1038 Solutions from GRACE. GFZ Data Services <http://doi.org/10.5880/icgem.2016.007>
1039 (2016).
- 1040 104. Bruinsma, S., Lemoine, J.-M., Biancale, R., & Vales, N. CNES/GRGS 10-day
1041 gravity field models (release 02) and their evaluation. *Adv. Space Res.*, **45**, 587-601,
1042 doi:10.1016/j.asr.2009.10.012 (2010).
- 1043 105. Kurtenbach, E., et al. Improved daily GRACE gravity field solutions using a
1044 Kalman smoother. *J. Geodynamics*, **59-60**, 39-48 (2012).
- 1045 106. Liu, X., et al. DEOS Mass Transport model (DMT-1) based on GRACE satellite
1046 data: methodology and validation. *Geophys. J. Int.*, **181**, 769-788, doi:10.1111/j.1365-
1047 246X.2010.04533.x (2010).
- 1048 107. Swenson, S., & Wahr, J. Post-processing removal of correlated errors in GRACE
1049 data. *Geophys. Res. Lett.* **33**, L08402, doi:10.1029/2005GL025285 (2006).
- 1050 108. Andrews, S. B., Moore, P., & King, M.A. Mass change from GRACE: a
1051 simulated comparison of Level-1B analysis techniques. *Geophys. J. Int.*, **200**, 503-
1052 518, doi:10.1093/gji/ggu402 (2011).
- 1053 109. Save H., Bettadpur, S., & Tapley, B.D. High resolution CSR GRACE RL05
1054 mascons. *J. Geophys. Res. Solid Earth*, **121**, 7547-7569, doi:10.1002/2016JB013007
1055 (2016).
- 1056 110. Landerer, F.W., Wiese, D.N., Bentel, K., Boening, C., & Watkins, M.M. North
1057 Atlantic meridional overturning circulation variations from GRACE ocean bottom
1058 pressure anomalies. *Geophys. Res. Lett.*, **42**, 8114-8121, doi:10.1002/2015GL065730
1059 (2015).
- 1060 111. Wiese, D. N., Yuan, D.-N., Boening, C., Landerer, F. W., & Watkins, M. M. *JPL*
1061 *GRACE Mascon Ocean, Ice, and Hydrology Equivalent Water Height RL05M.1 CRI*
1062 *Filtered Version 2*. PO.DAAC, CA, USA. doi:10.5067/TEMSC-2LCR5 (2016).
- 1063 112. Wiese, D.N., Landerer, F.W., & Watkins, M.M. Quantifying and reducing
1064 leakage errors in the JPL RL05M GRACE mascon solution. *Water Resour. Res.* **52**,
1065 7490-7502, doi:10.1002/2016WR019344 (2016).
- 1066 113. Cheng, M. & Tapley, B. D. Variations in the Earth's oblateness during the past 28
1067 years. *J. Geophys. Res.* **109**, B09402 (2004).
- 1068 114. Swenson, S., Chambers, D., & Wahr, J. Estimating geocenter variations from a
1069 combination of GRACE and ocean model output. *J. Geophys. Res.* **113**, B08410,
1070 doi:10.1029/2004JB003028 (2008).
- 1071 115. Ivins E.R. *et al.* Antarctic contribution to sea level rise observed by GRACE with
1072 improved GIA correction, *J. Geophys. Res.* **118**, 3126-3141, doi:10.1002/jgrb.50208
1073 (2013).
- 1074 116. Shepherd, A., et al. A reconciled estimate of ice-sheet mass balance. *Science*, **338**,
1075 1183-1189, doi:10.1126/science.1228102 (2012).
- 1076 117. Wahr, J., Nerem, R. S., & Bettadpur, S. V. The pole tide and its effect on GRACE
1077 time variable gravity measurements: Implications for estimates of surface mass
1078 variations. *J. Geophys. Res. Solid Earth* **120**, 4597-4615, doi:10.1002/2015JB011986
1079 (2015).

- 1080 118. Fagiolini, E., Flechtner, F., Horwath, M., & Dobslaw, H. Correction of
1081 inconsistencies in ECMWF's operational analysis data during de- aliasing of GRACE
1082 gravity models. *Geophys. J. Int.* **202**, 2150–2158, doi:10.1093/gji/ggv276 (2015).
- 1083 119. Scanlon, B.R. *et al.* Global evaluation of new GRACE mascon products for
1084 hydrologic applications. *Water Resour. Res.*, **52**, 9412-
1085 9429http://dx.doi.org/10.1002/2016WR019494 (2016).
- 1086 120. Chen, J.L., Wilson, C.R., Tapley, B.D., Save, H., & Cretaux, J.-F. Long-term and
1087 seasonal Caspian Sea level change from satellite gravity and altimeter measurements.
1088 *J. Geophys. Res. Solid Earth*, **122**, 2274-2290, doi:10.1002/2016JB013595 (2017).
- 1089 121. A, G., Wahr, J. & Zhong, S. Computations of the viscoelastic response of a 3-D
1090 compressible Earth to surface loading: An application to Glacial Isostatic Adjustment
1091 in Antarctica and Canada. *Geophys. J. Int.* **192**, 557–572, doi:10.1093/gji/ggs030
1092 (2013).
- 1093 122. Paulson, A., Zhong, S., & Wahr, J. Inference of mantle viscosity from GRACE
1094 and relative sea level data. *Geophys. J. Int.* **171**, 497–508, doi:10.1111/j.1365-
1095 246X.2007.03556.x (2007).
- 1096 123. Purcell, A., Tregoning, P., & Dehecq, A. An assessment of the *ICE6G_C(VM5a)*
1097 glacial isostatic adjustment model. *J. Geophys. Res. Solid Earth* **121**, 3939–3950,
1098 doi:10.1002/2015JB012742 (2016).
- 1099 124. Purcell, A., Tregoning, P., & Dehecq A. Reply to comment by W. R. Peltier, D. F.
1100 Argus, and R. Drummond on “An assessment of the *ICE6G_C (VM5a)* glacial
1101 isostatic adjustment model. *J. Geophys. Res. Solid Earth* **122**,
1102 doi:10.1002/2017JB014930 (2017).
- 1103 125. Landerer, F.W., and Swenson, S.C. Accuracy of scaled GRACE terrestrial water
1104 storage estimates. *Water Resour. Res.*, **48**, W04531, doi:10.1029/2011WR011453
1105 (2012).
- 1106 126. Rodell, M., et al. The global land data assimilation system. *Bull. Amer. Meteorol.*
1107 *Soc.* **85**, 381-394, doi:10.1175/BAMS-85-3-381 (2004).
- 1108 127. Crétaux, J.-F., et al. SOLS: A lake database to monitor in the near real time water
1109 level and storage variations from remote sensing data. *Adv. Space Res.* **47**,
1110 1497-1507, doi:10.1016/j.asr.2011.01.004 (2011).
- 1111 128. Avakyan A.B. Volga-Kama cascade reservoirs and their optimal use. *Lakes &*
1112 *Reservoirs Research & Management* **3**, 113-121, doi:10.1111/j.1440-
1113 1770.1998.tb00038.x (1998).
- 1114 129. OECD, Crop production (indicator). doi:10.1787/49a4e677-en. Accessed online
1115 at <https://data.oecd.org/agrooutput/crop-production.htm> (2017).
- 1116 130. Gelaro, R., et al. The modern-era retrospective analysis for research and
1117 applications, version 2 (MERRA-2). *J. Clim.* **30**, 5419-5454, doi:10.1175/JCLI-D-16-
1118 0758.1 (2017).
- 1119 131. Farinotti, D. *et al.* Substantial glacier mass loss in the Tien Shan over the past 50
1120 years. *Nature Geoscience* **8**, 716-722, doi:10.1038/ngeo2513 (2015).
- 1121 132. Gardner, A. et al. A reconciled estimate of glacier contributions to sea level rise:
1122 2003 to 2009. *Science* **340**, 852-857, doi:10.1126/science.1234532 (2013).
- 1123 133. Mou, D. & Li, Z. A spatial analysis of China's coal flow. *Energy Policy* **48**, 358-
1124 368, doi:10.1016/j.enpol.2012.05.034 (2012).

- 1125 134. Feng, W. *et al.* Evaluation of groundwater depletion in North China using the
1126 Gravity Recovery and Climate Experiment (GRACE) data and ground-based
1127 measurements. *Water Resour. Res* **49**, 2110-2118, doi:10.1002/wrcr.20192 (2013).
1128 135. Moiwo, J. P., Tao, F., & Lu, W. Analysis of satellite-based and in situ hydro-
1129 climatic data depicts water storage depletion in North China Region. *Hydrological*
1130 *Proc.* **27**, 1011-1020, doi:10.1002/hyp.9276 (2013).
1131 136. Tang, Q., Zhang, X., & Tang, Y. Anthropogenic impacts on mass change in North
1132 China. *Geophys. Res. Lett.* **40**3924-3928, doi:10.1002/grl.50790 (2013).
1133 137. Ebead, B., Ahmed, M., Niu, Z., & Huang, N. Quantifying the anthropogenic
1134 impact on groundwater resources of North China using Gravity Recovery and
1135 Climate Experiment data and land surface models. *J.Applied Remote Sensing* **11**,
1136 026029-026029, doi:10.1117/1.JRS.11.026029 (2017).

1137 **Extended Data Captions**

1138 **Figure ED1. Non-seasonal TWS anomalies: global regions.** Time series of
1139 monthly TWS anomalies (departures from the period mean) from GRACE, after
1140 removing the mean seasonal cycle, averaged over each of study regions 1-6 (panels
1141 a-f), as equivalent heights of liquid water (cm). Note that the y-axes vary among
1142 panels.

1143 **Figure ED2. Non-seasonal TWS anomalies: Eurasia.** As in Figure ED1, for
1144 regions 7-18 (panels a-l).

1145 **Figure ED3. Non-seasonal TWS anomalies: North and South America.** As in
1146 Figure ED1, for regions 19-26 (panels a-h).

1147 **Figure ED4. Non-seasonal TWS anomalies: Africa and Australia.** As in Figure
1148 ED1, for regions 27-34 (panels a-h).

1149 **Figure ED5. Annual precipitation totals: global regions.** Time series of annual
1150 precipitation totals (mm) averaged over each of study regions 1-6 (panels a-f), based
1151 on GPCP v.2.3. Note that the y-axes vary among panels.

1152 **Figure ED6. Annual precipitation totals: Eurasia.** As in Figure ED5, for regions 7-
1153 18 and the full drainage basins of the Aral and Caspian Seas (panels a-n).

1154 **Figure ED7. Annual precipitation totals: North and South America.** As in Figure
1155 ED5, for regions 19-26 (panels a-h).

1156 **Figure ED8. Annual precipitation totals: Africa and Australia.** As in Figure ED5,
1157 for regions 27-34 (panels a-h).

1158 **Figure ED9. Comparison of TWS trends (cm/yr) over India (January 2003 -**
1159 **March 2016) from three GRACE mascon solutions.** JPL-M 3° (panel a), CSR-M 1°

1160 (b), GSFC-M 1° (c), and JPL-M smoothed with a 200 km radius Gaussian filter and plotted
1161 at 1° (d). Notice the similarity between the latter three trend maps, whose regional trend
1162 amplitudes have all been dampened by smoothing.

1163 **Figure ED10. Comparison of normalized anomalies of Caspian Sea level**
1164 **changes and three primary drivers.** Normalized anomalies of (1) changes in
1165 annual mean Caspian Sea level, (2) Volga River discharge, (3) Russian total crop
1166 weight, and (4) Caspian Sea evaporation. Precipitation (Figure ED2) is the other
1167 primary driver. Sea level change is positively correlated with Volga River discharge
1168 is and negatively correlated with Russian crop weight and evaporation.

1169

1170

1171 **Figures**

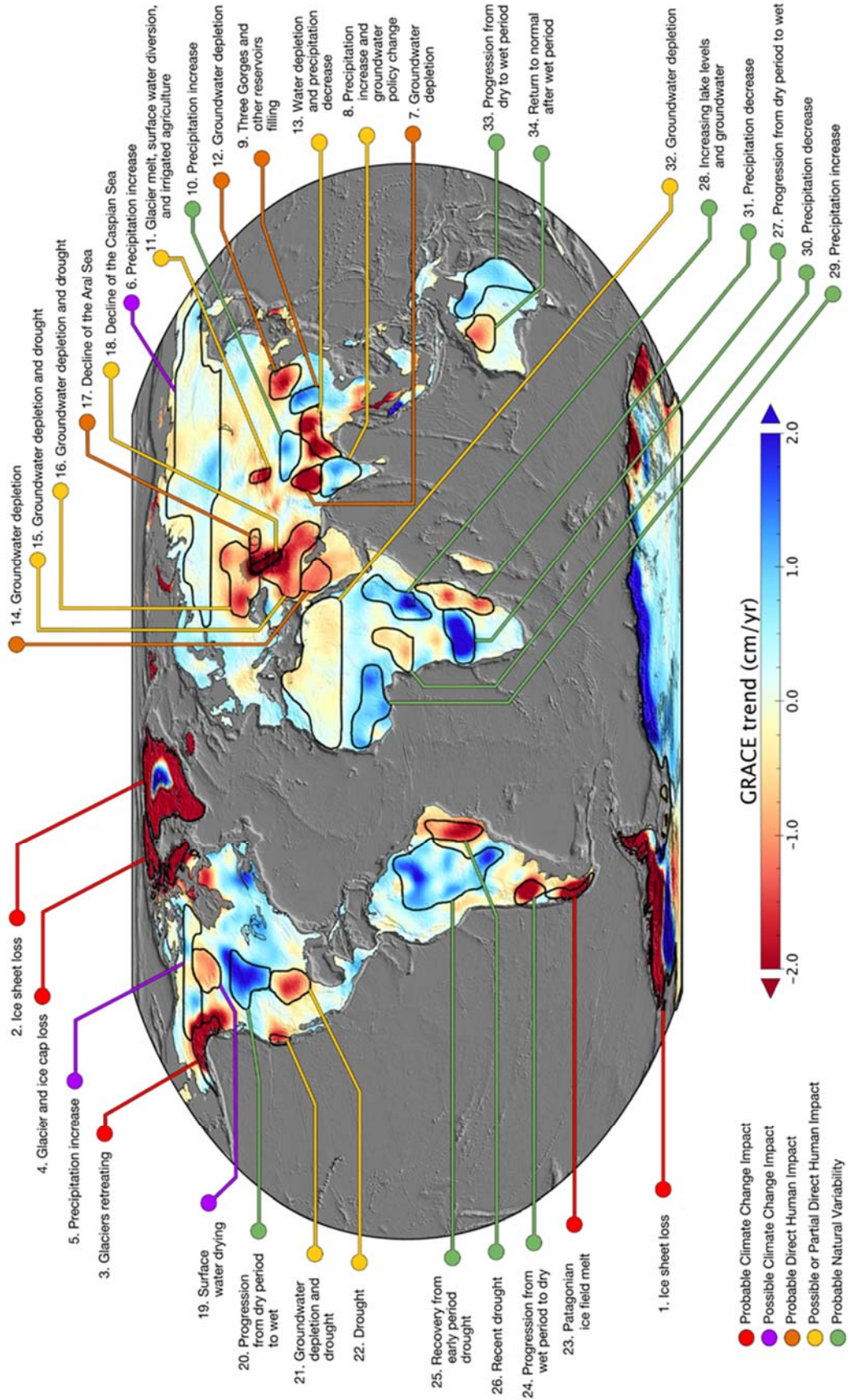
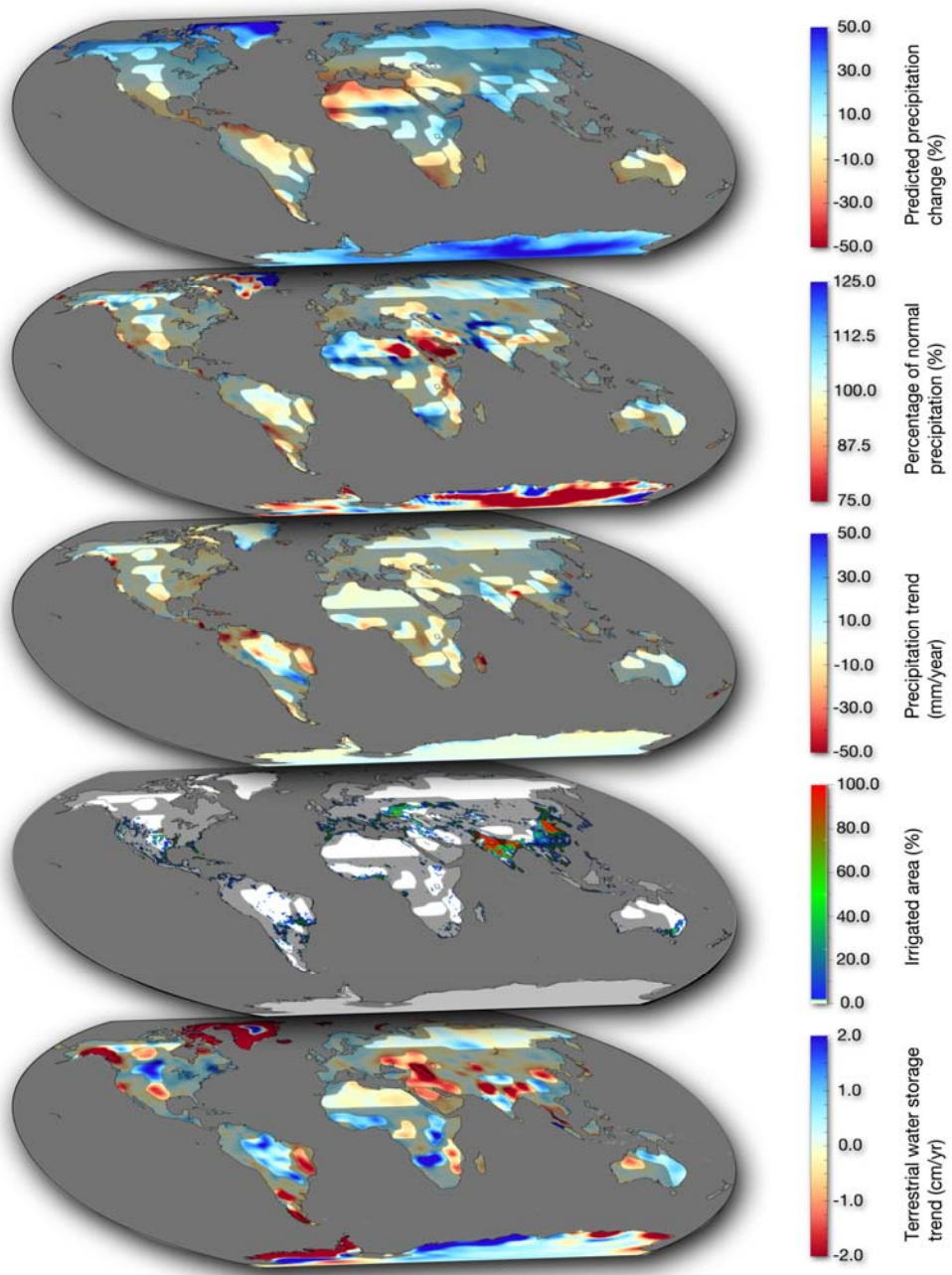


Figure 1



1173

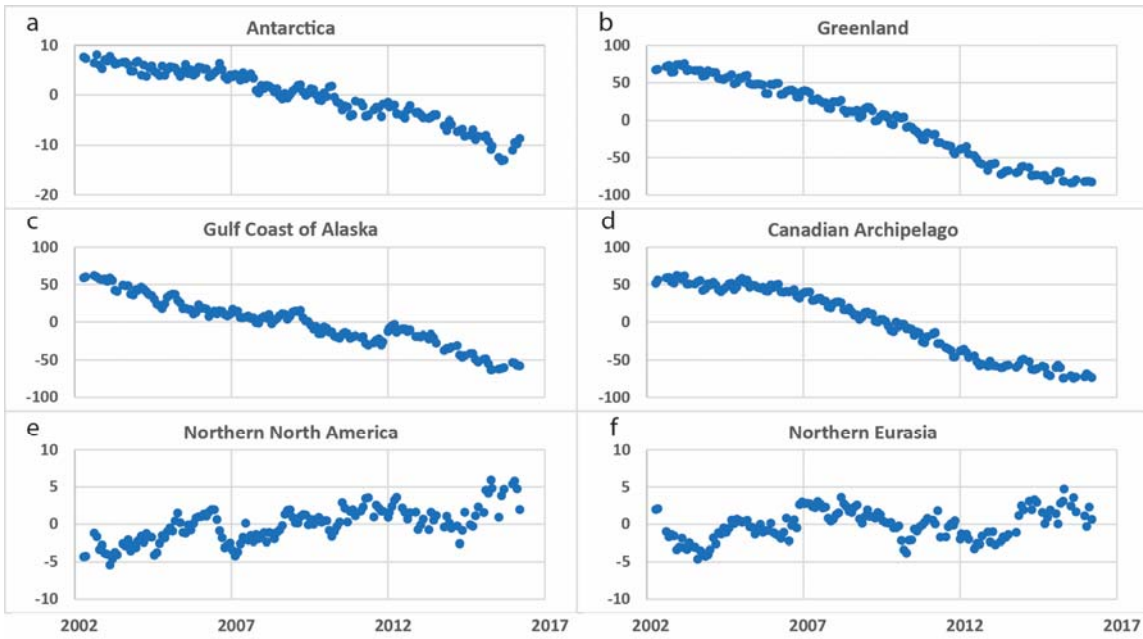
1174

Figure 2

1175

1176 **Extended Data Figures**

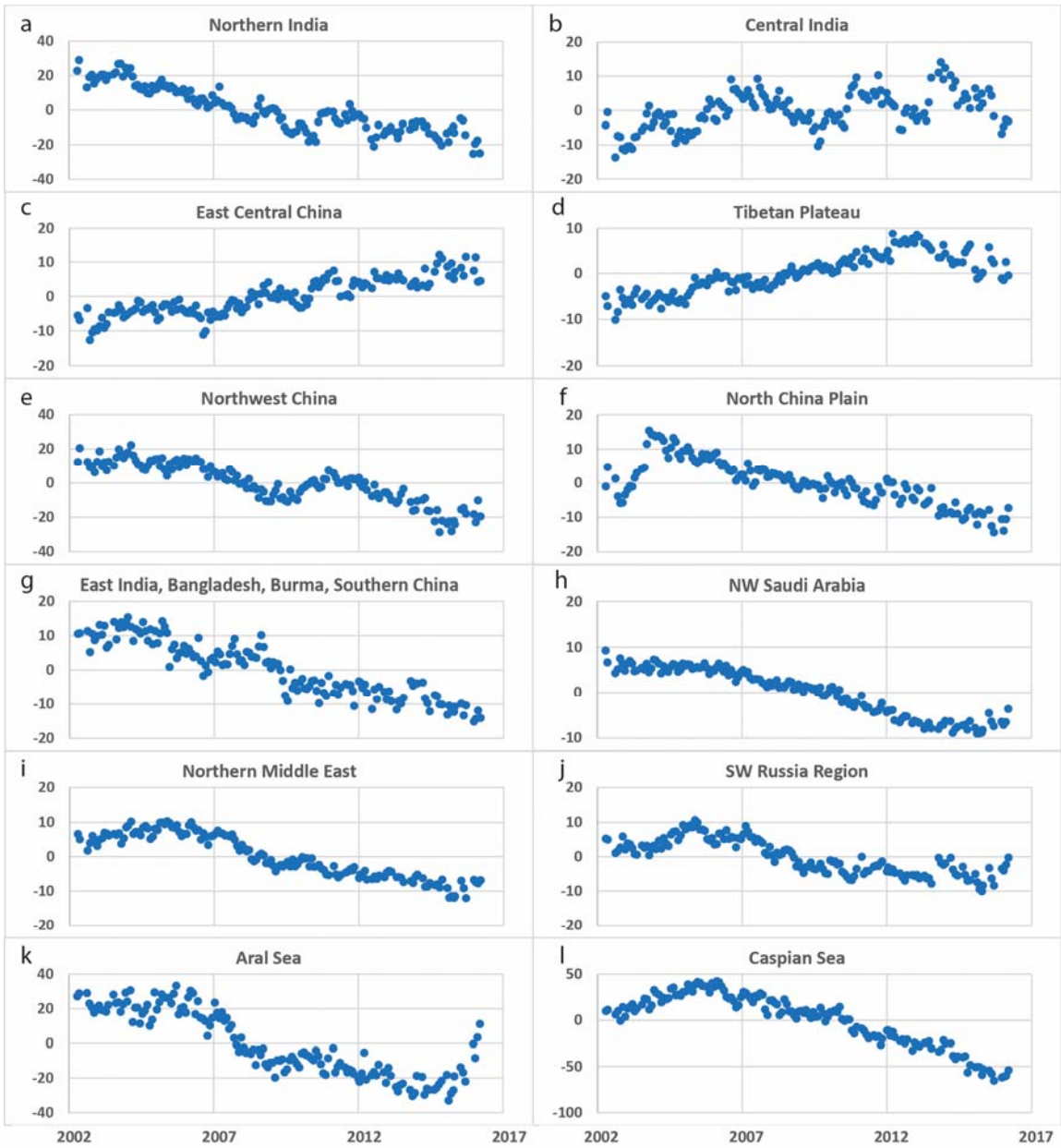
1177



1178

1170

Figure ED1



1181
1182

Figure ED2

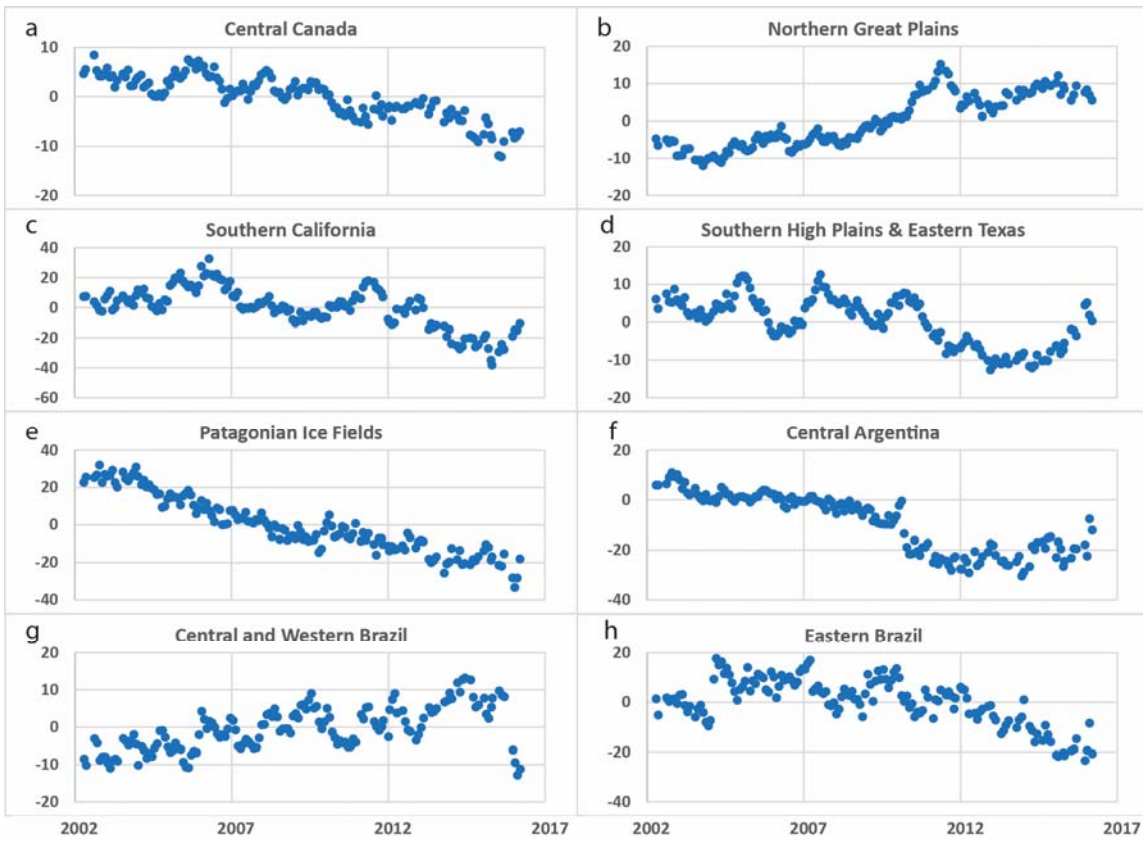
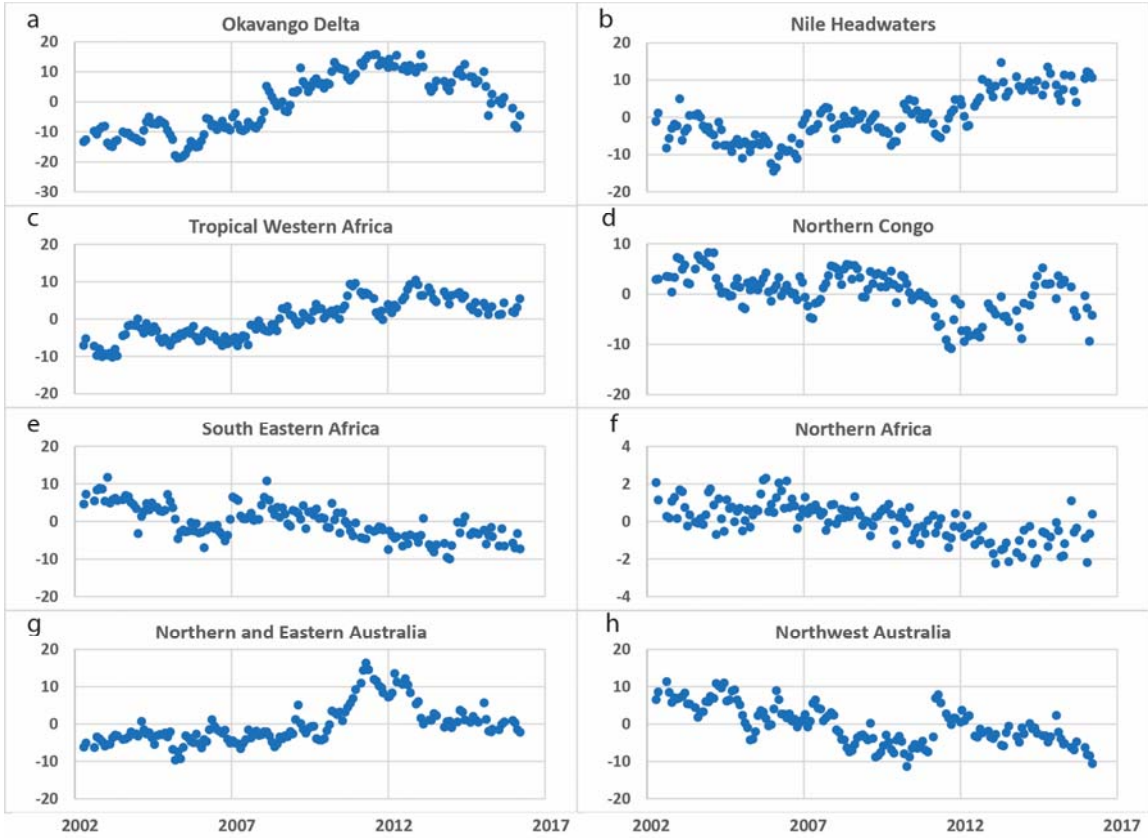


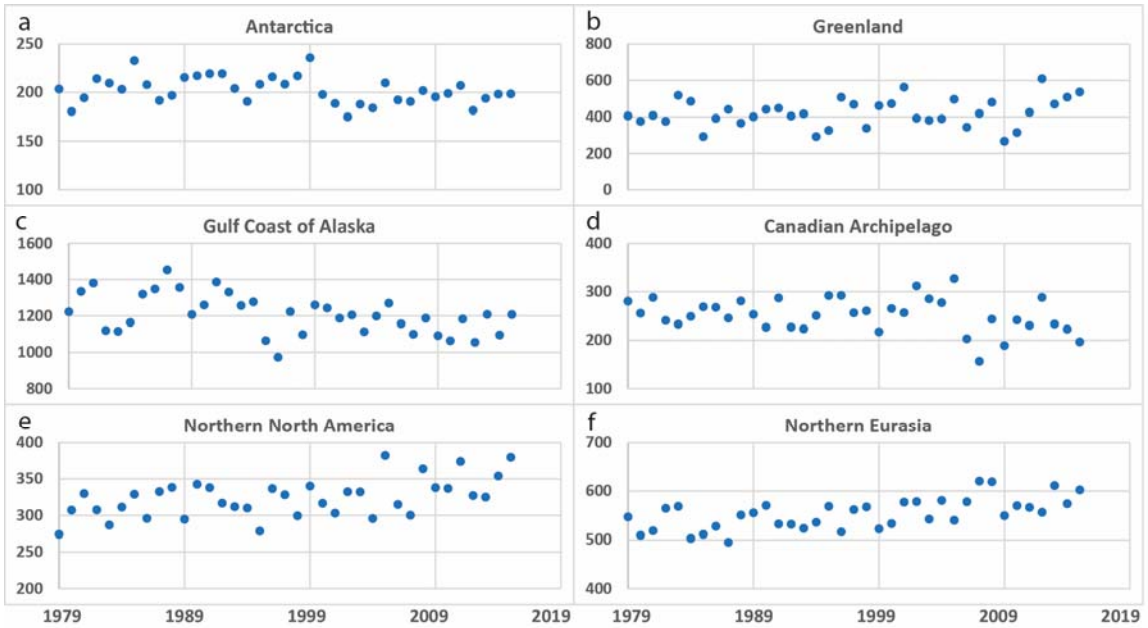
Figure ED3



1187

1188

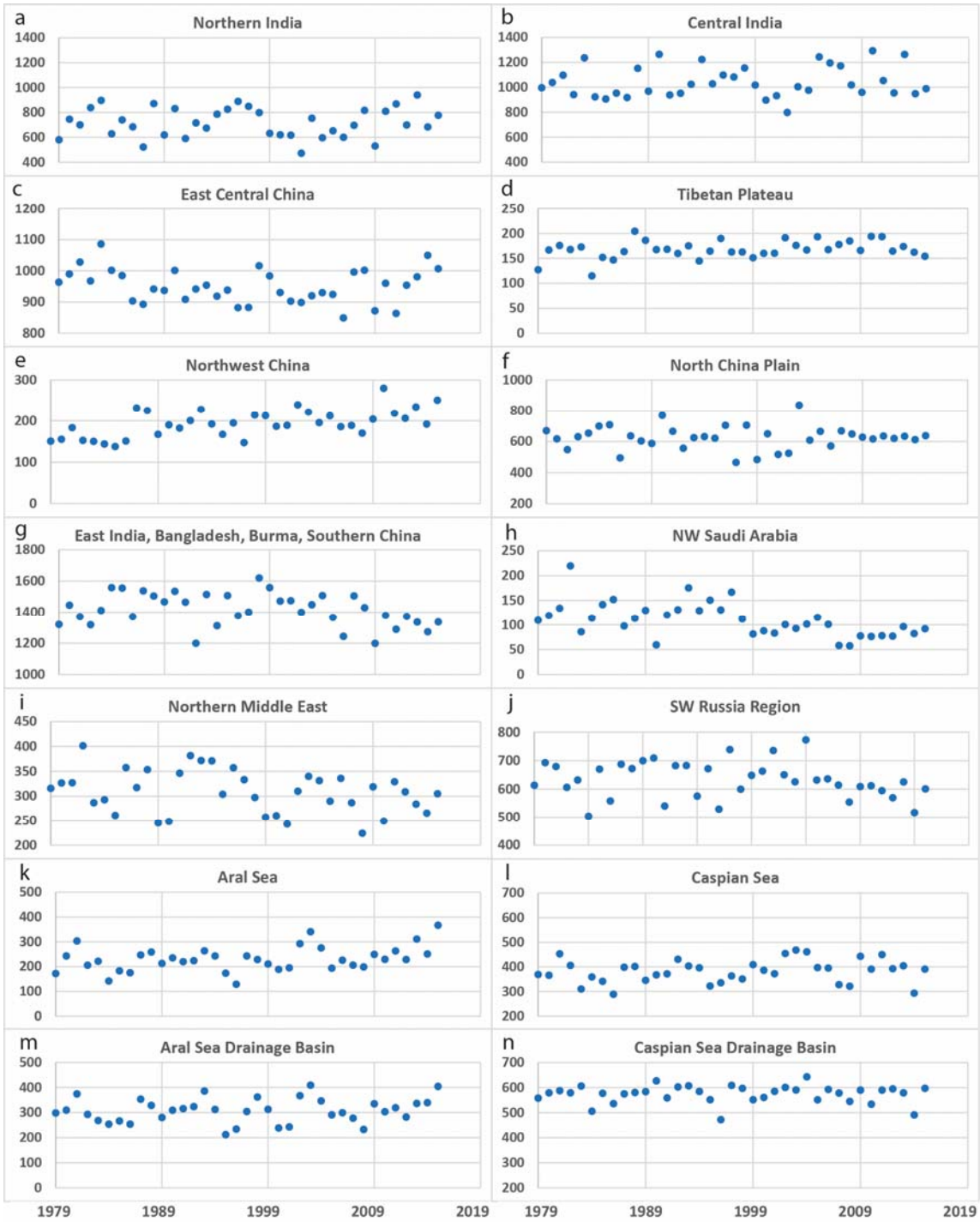
Figure ED4



1191

1192

Figure ED5

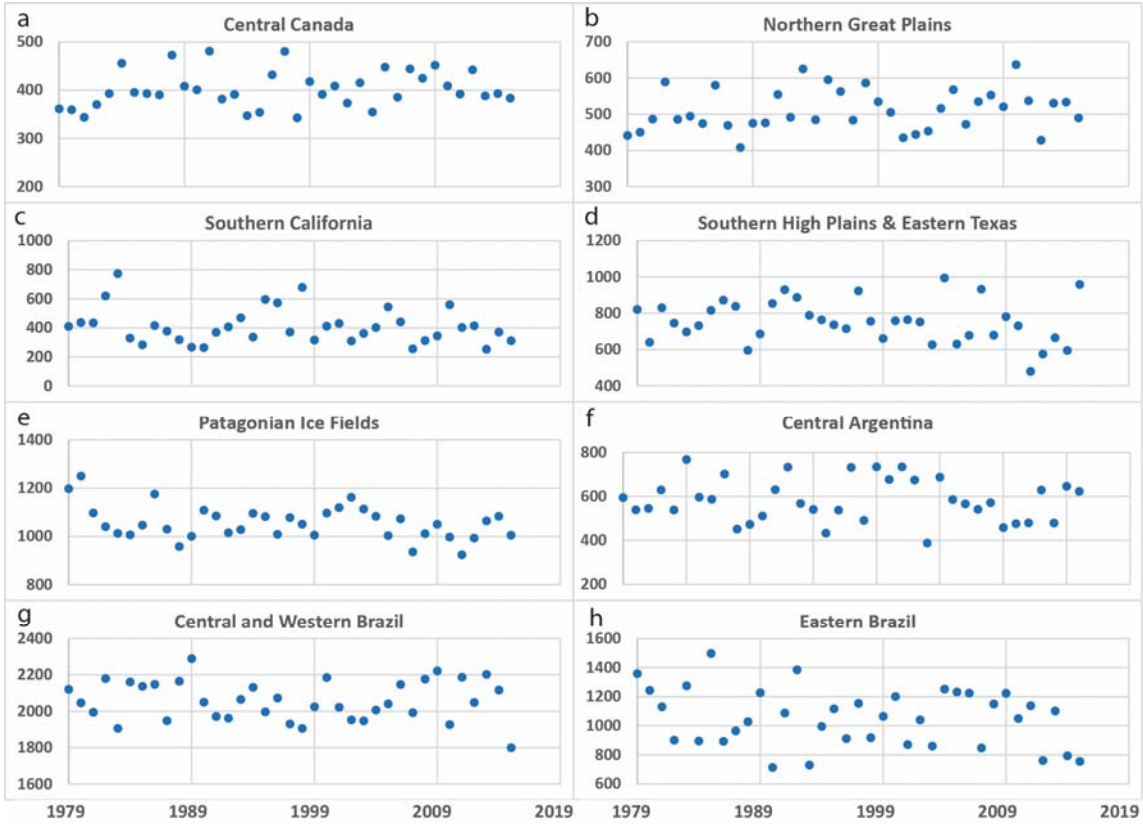


1194

1195

Figure ED6

1197



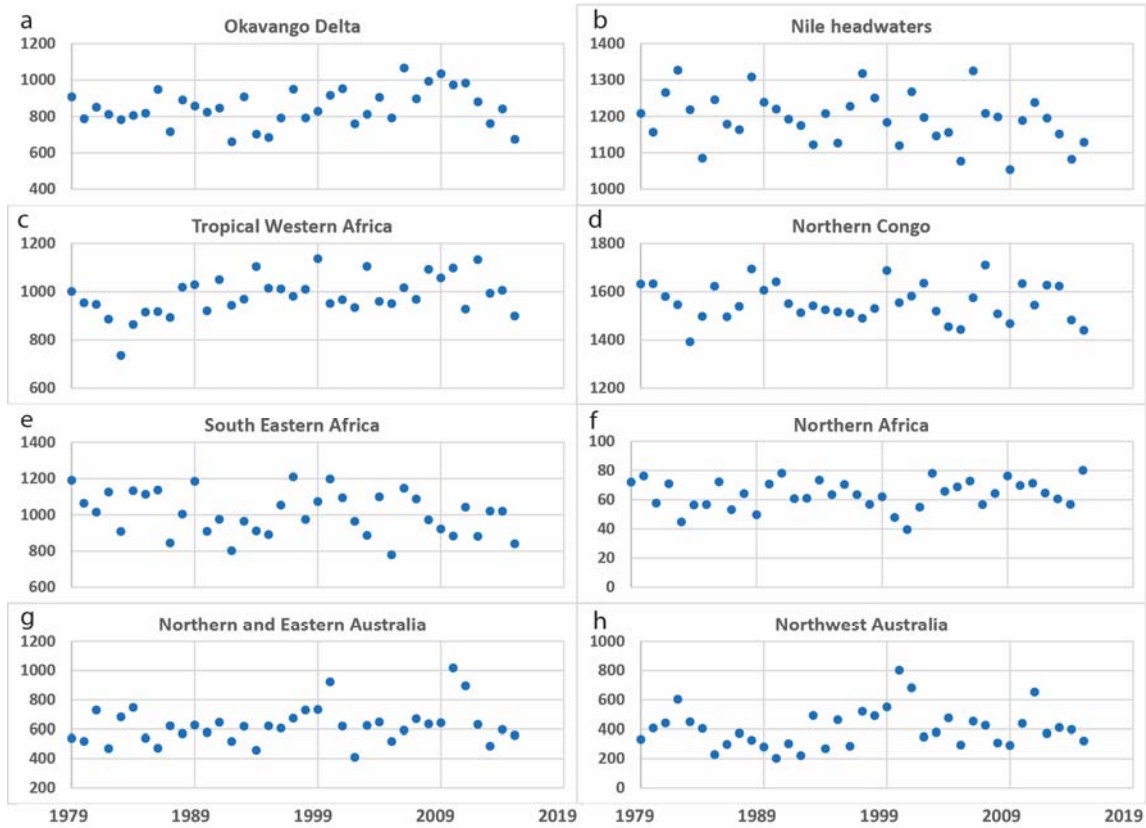
1198

1199

Figure ED7

1202

1203



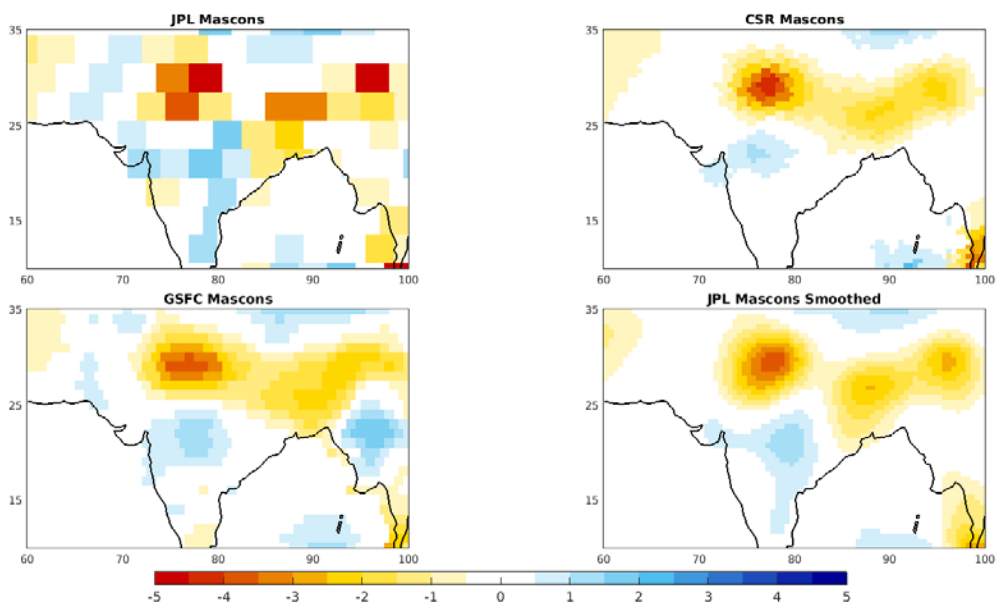
1204

1205

Figure ED8

1207

1208



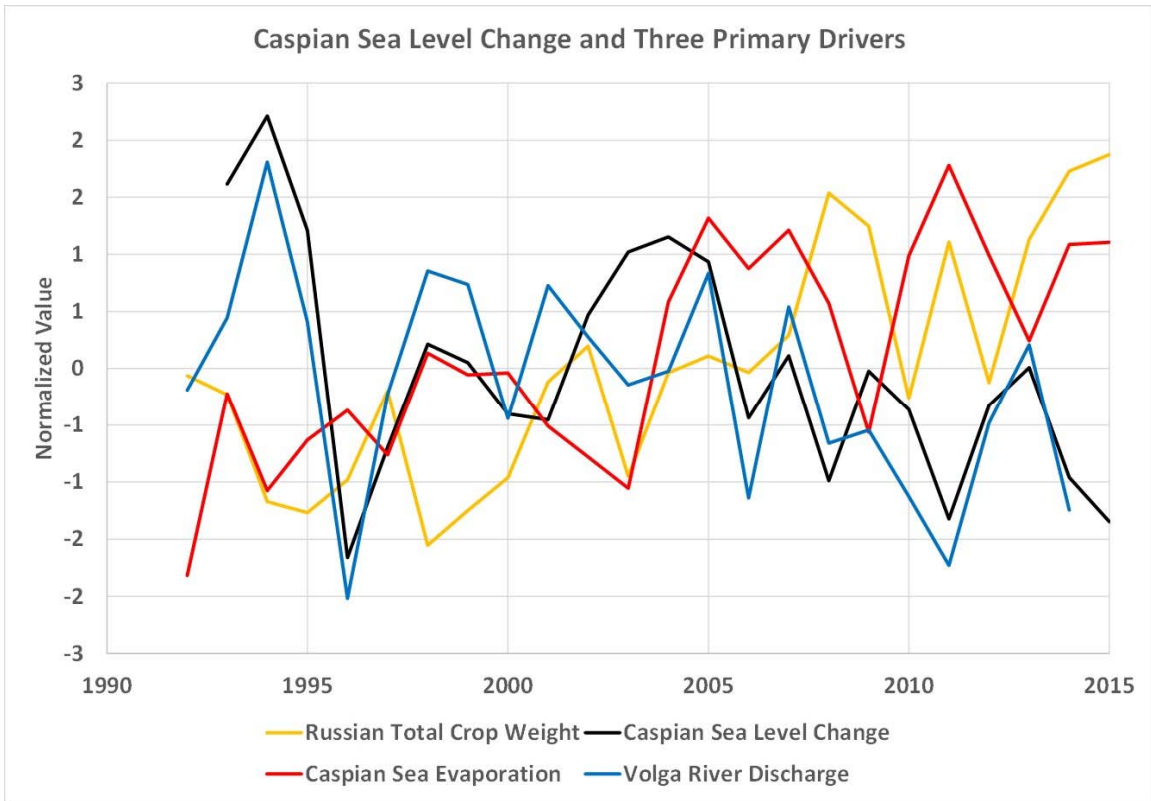
1209

1210

1211

Figure ED9

1212



1213
1214

Figure ED10

CORRECTIONS & AMENDMENTS

CORRECTION

<https://doi.org/10.1038/s41586-018-0831-6>

Author Correction: Emerging trends in global freshwater availability

M. Rodell, J. S. Famiglietti, D. N. Wiese, J. T. Reager, H. K. Beaudoin, F. W. Landerer & M.-H. Lo

Correction to: *Nature* <https://doi.org/10.1038/s41586-018-0123-1>, published online 16 May 2018.

In Fig. 2 of this Analysis, the tick-mark labels on the colour bars in the second and third images from the top were inadvertently swapped. In addition, the citation at the end of the sentence, “On a monthly basis GRACE can resolve TWS changes with sufficient accuracy over scales that range from approximately 200,000 km² at low latitudes to about 90,000 km² near the poles” should be to ref. ⁴ not ref. ¹. These errors have been corrected online.